

Response to comments of Kirill Gerke on the manuscript “Combined numerical and experimental study of microstructure and permeability in porous granular media” by Philipp Eichheimer et al., se-2019-199.

We thank Kirill Gerke for his great review. His constructive and useful comments that helped us to improve our manuscript.

Please find below a point by point response to the comments (comments of the reviewer in black and our response in [blue](#)).

Sincerely,
Philipp Eichheimer on behalf of the authors

The paper is interesting and follows logically from the previous paper of the same main Author. If I understood correctly, the paper was not accepted for review by 3 potential reviewers and for this reason finally ended up with me (again). I found the idea of lab experiment and pore-scale simulations to be very relevant, we do lack such studies. But while reading this manuscript more deeply i was somewhat taken aback by Kozeny-Carman relationships the Authors use. While I find lab vs. modelling work to be very important and do support this paper to be published with SE (after some re-branding), i regret to say that I have a major point of criticism here as well. It really puzzles me why would modern researchers utilize Kozeny-Carman relationship and why everybody at some point want to establish some kind of K-C relationship? How useful is that? We know very well already that what works for spheres does not work for real porous media samples. Moreover, the concept of hydraulic tortuosity, while still popular, provides very low information bulk measure of flow velocity field (as Authors show depending on the methodology to compute tau, the results are quite different). It may be so that computed tau values are interesting to show that they are different from previously computed, this again provides close to zero scientific value. So, while Authors proposed a “novel” Kozeny-Carman model, my question – how is it even useful, practical or simply scientifically valuable? This puts the conclusion

for this work into a state of not really going anywhere. If compared against lab measurements or simulations K-C produces orders of magnitude errors, as is evident from your figures. To relate to previous results for spheres or another K-C relationship you could refer to: Martys, N. S., Torquato, S., & Bentz, D. P. (1994). Universal scaling of fluid permeability for sphere packings. *Physical Review E*, 50(1), 403. Garcia, X., Akanji, L. T., Blunt, M. J., Matthai, S. K., & Latham, J. P. (2009). Numerical study of the effects of particle shape and polydispersity on permeability. *Physical Review E*, 80(2), 021304. Now, around lines 270-275 you discuss why the results of permeability for simulations are different from these of lab measured values. While you mention that size and boundary effects could influence your results (for such small volumes i would warily estimate an error due to boundary condition to be up to 20-50%, and in this regard you could refer to Gerke, K. M., Karsanina, M. V., & Katsman, R. (2019). Calculation of tensorial flow properties on pore level: Exploring the influence of boundary conditions on the permeability of three-dimensional stochastic reconstructions. *Physical Review E*, 100(5), 053312), i think the main reason is different. As you can see from figure 2 you have very high porosity contrast along z-axis. Now, if you have 0.05 porosity down there – this part will dominate the porosity for the whole sample. This makes sense, as you lab values are always lower. What i would do with your (really good!) data? I would leave all this K-C and tortuosity thing, but rewrite it as not useful and your data clearly shows that (which is, again, good). Now, you could assemble all these small pieces of 3D images you modelled with FDM solver into a 3d matrix of permeability values and upscale it (as simply as harmonic means should do the trick i suppose) to compare again the lab. This could lead to something interesting – at least you would be able to show how different model and lab values are. You could use these simple upscaling schemes as inspiration: Jang, J., Narsilio, G. A., & Santamarina, J. C. (2011). Hydraulic conductivity in spatially varying media - a pore-scale investigation. *Geophysical journal international*, 184(3), 1167-1179. With this little addition you paper could be completely rebranded from meaningless K-C to something really relevant to our field (kind of full core comparison between lab and modelling). Hope this helps and does not introduce too much addition work. Otherwise it is very hard for me to accept the paper

as is - i think we have to automatically reject all papers dealing with K-C (just because it is wasting of time, money, pages, you name it). Thank you for your detailed comment regarding the usage of the Kozeny-Carman relation. We rebranded and restructured our manuscript as suggested in your comment to not only focus on the Kozeny-Carman relation. We refrained from completely removing the Kozeny-Carman equation from the paper, as it is still frequently used in different scientific areas.

Instead, we now evaluate different published permeability parameterizations. We find that the modified Kozeny-Carman equation and the parameterization by Martys et al., 1994 provide a similarly good fit to the numerical and experimental permeability values, but also that they fail to capture second-order microstructural effects. We also incorporated your comment on permeability upscaling and now report permeabilities not per subsample, but as the geometric mean of all subsamples.

In the methods section we now also discuss your comment regarding the minimum effective porosity controlling the permeability entire sample and modified figure 5 to account for the minimum effective porosity. We decided to keep the results on hydraulic tortuosity in the manuscript as the parameter of hydraulic tortuosity is quite important not only for the Kozeny-Carman relation but is highly interesting for several engineering disciplines.

1. Table 1 – is porosity measured (as computed from mass and volume?) or computed from images? How A is computed? Do all samples have the same trends in porosity as in Fig.2, if so, does porosity represent an average for the whole cylinder?

1) The porosity in our study is computed from the obtained CT-images only. An experimental technique using a pycnometer, as suggested by reviewer #2, is not possible as we do not have access to such a device.

2) The cross-sectional area A we used to determine permeability is obtained using ImageJ.

3) Nearly all samples show a densification trend in porosity. Only samples with very low porosity do not show densification. Reported porosities are averages for the whole cylinder. We now also report the minimum effective porosity for each sample.

2. 2.6 – do you state that you use ϕ_{eff} for all later computations as porosity? If so, please, make it easier to guess.

Thank you for this remark. We now state this issue more clearly (Page 8, line 160 ff.).

3. 2.7 – how do you compute the area? By voxel counting and summarizing the interface as voxel faces?

We computed the area of an isosurface from the CT images using MatLab. In detail we compute an isosurface of the binary images and then the area of the resulting isosurface.

4. Eq.10-11 and Eq.12 utilize different V_b and V_B values but i guess refer to the same volume.

We corrected the equations.

5. Not clear why you report Eq.14-17 if you use Eq.13 (which seems to me to be superior as it calculates hydraulic tortuosity using streamlines instead of lausy porosity-based relationships).

As the computation and interpretation of the hydraulic tortuosity is still under debate we wanted to give a brief overview for the reader, which relations have been proposed by other authors to which we compare our results later in figure 4. We specifically wanted to show that the porosity-based relationships do not perform well compared to our data.

6. 3.2 – your model is basically the same as of Koponen. The scatter is huge, is there any point in using such relationships? (Later I see you also substitute the points instead of this relationship, but I do not see the difference between them, is there any?)

This is a good point. We now only use the arithmetic average of the tortuosity as an input for the Kozeny-Carman equation. We also noted that using either a fit to the porosity-tortuosity relationship by Koponen or an arithmetic average only have a minor effect on predicted permeabilities. However, as hydraulic tortuosity itself (besides its potential effect on permeability) is of interest in different scientific fields, we think it is important to report our results here.

7. Eq.23 have simply tau, not tau_H (as i guess it should be?).

We corrected this mistake.

8. around line 230: sorry, but i could not follow your explanation of critical exponent through, including this paragraph and also appendix D. How did you evaluated phi_c?

We based the critical porosity threshold on porosity measurements of the samples used in our study. By systematically analyzing each sample we observed that for samples below 1% porosity we did not find any connected cluster, while samples with porosities slightly higher than 1% contained a percolating cluster. For this reason, we employed a critical porosity threshold of 0.01 instead of the published value of 0.03. As the additional description provided in Appendix D was not specifically concerned with this issue, but rather with a general explanation on why a critical porosity threshold exists, we chose to remove the appendix and the corresponding figure, as this caused too much confusion.

9. Could you, please, also describe the sample preparation procedure a bit more, in particular how do you wrap it into resin? I could not get it completely from the current description.

Thank you for your comment. In a first step we wrap the sintered glass bead sample into a high viscous resin. This can be done as this resin has a very high viscosity and can be deformed

by hand. For this reason the sintered glass bead sample is literally wrapped or rolled into the resin. Just the top and bottom surface, which are needed for the experimental permeability measurements are left open. After drying, the glass bead sample with the attached highly viscous resin is embedded into a low viscous resin to create a surface, which can be sealed during the experiments. To avoid any leaks between the sample and the attached O-rings of the permeameter, both surfaces, top and bottom, are polished.

Please find the revised manuscript with highlighted changes in the supplement.

Response to comments of an anonymous referee on the manuscript "Combined numerical and experimental study of microstructure and permeability in porous granular media" by Philipp Eichheimer et al., se-2019-199.

We thank the anonymous referee for his review. His constructive comments helped us to improve our manuscript.

Please find below a point by point response to the comments (comments of the reviewer in black and our response in blue).

Sincerely,
Philipp Eichheimer on behalf of the co-authors

1. In the abstract, the authors stress the importance of characterizing fluid flow at different scales, and they state their study can be used to simulate permeability in large-scale numerical modelling. However, the up-scale of the results and the limitations of the proposed approach are never properly discussed. Therefore, it is difficult to understand how and to what extent the permeability prediction proposed in this paper is applicable to large scale modelling.

Thank you for this comment. The proposed permeability parameterizations can be used to predict permeability on the large-scale using numerical simulations. For this reason the parameterizations are useful for isotropic low porosity media e.g. sandstones. In nature rocks mostly consists of various grain shapes and sizes, for which the proposed parameterizations are only partially valid. We now discuss this issue in the manuscript (p. 18, line 381 ff.)

2. It is not clear how the porosity of the sintered samples is evaluated. Only through CT-scan analysis? If so, could the authors measure it experimentally (e.g., pycnometer)? This would give a measure of the effective porosity of the samples and could be compared to the computed one.

Moreover, how is the porosity reported in table 1 evaluated, both total and effective? From Figure 2, the porosity in a single sample changes quite a lot from $\sim 5\%$ to $\sim 20\%$ (and the reported value in table 1 is $\sim 13\%$). During permeability experiments, the low porosity zone at the bottom of the samples controls the overall permeability values resulting in a shift of the points toward higher porosity values in the permeability versus porosity plot (i.e., Figure 5). This could explain the discrepancy between computed permeability using subsamples and measured permeability of the entire sample. Could the authors add in Table 1 the minimum porosities for all the samples (or report in the supplementary material all the curves showing the height of samples versus porosities)? Could the authors plot the measured permeability versus the minimum porosity in Figure 5?

Furthermore, what is the size of subsamples in z direction? Could the author clarify it in the main text?

Thank you for this comment. The porosity is only measured from the obtained CT-scans. Unfortunately, we do not have access to a pycnometer and therefore it is not possible to provide experimental porosity values.

The effective porosity represents all connected void clusters which contribute to the fluid flow and therefore permeability. The total porosity also takes into account inclusions and clusters which are not connected to the top and bottom of the sample.

We agree that permeability may not necessarily be affected by the total effective porosity, but rather by the minimum effective porosity in a sample (in a slice perpendicular to the flow direction). We therefore also report the minimum effective porosity of each sample and added the values in table 1 and changed figure 5 to plot permeability against the minimum effective porosity.

The height of the sample in z-direction is reported in table 1 and is around 5 mm.

3. In figure 4b, the relation proposed by Koponen et al. (1996) seems to fit the data similarly to the relations proposed by the authors (Figure 4d). If I understand properly, the authors

justify the choice arguing that the fits presented in Figure 4a, b and c have negative or low R^2 values. However, they write that also the fit shown in Figure 4d has a low R^2 . The R^2 values for the fits in Figure 4 are not reported in the main text. Thus, it is difficult for the reader to understand why the fit in Figure 4d is better than the fit in Figure 4c. Could the authors add this information in the main text? Could the authors clarify why they do not use Koponen et al. (1996) hydraulic tortuosity-porosity relation?

Thank you for this comment. We added R^2 values to all plots for the hydraulic tortuosity.

In general, all of the proposed relations for hydraulic tortuosity do not show good agreement, in particular the ones proposing an strong increase in hydraulic tortuosity when the critical porosity is approached. The relation of Koponen et al. (1996) shows that that the value of hydraulic tortuosity does not change significantly with different porosities, thus representing a similar trend to our data. As all fits, represented by a low R^2 value, do not properly fit our data we used the arithmetic mean of all calculated hydraulic tortuosities for the permeability parameterization.

4. The sentence “We determine flow properties like hydraulic tortuosity and permeability using both experimental measurements and numerical simulations.” could be misleading. Hydraulic tortuosity is not determined by experimental measurement. Could the authors clarify it?

This is correct, the old formulation was misleading. We modified the corresponding sentences as hydraulic tortuosity and permeability are computed numerically and the experimental permeability measurements are used to verify the obtained parameterization. (p.1, line 6 ff.)

5. Could the authors define the hydraulic radius?

We now give a definition for the hydraulic radius. (p.12, line 252)

6. Is the hydraulic radius constant? Is it not affected by different porosities?

The hydraulic radius only depends on grain size, which controls the effective pore volume between adjacent grains and is thus rather a pore-specific than a volume-specific property. As our samples consist of sintered glass bead packings with a relatively narrow grain size distribution, pore sizes throughout the sample do not vary significantly and thus also not the hydraulic radius. During sintering, some of these pores are closed, but the remaining pores do not significantly change their size. For this reason, the hydraulic radius also remains approximately constant.

7. Could the authors add R^2 values in the text?

We added the corresponding R^2 values to the plots of hydraulic tortuosity.

Please find the revised manuscript with highlighted changes in the supplement.

Combined numerical and experimental study of microstructure and permeability in porous granular media

Philipp Eichheimer¹, Marcel Thielmann¹, Wakana Fujita², Gregor J. Golabek¹, Michihiko Nakamura², Satoshi Okumura², Takayuki Nakatani², and Maximilian O. Kottwitz³

¹Bayerisches Geoinstitut, University of Bayreuth, Universitätsstrasse 30, 95447 Bayreuth, Germany

²Department of Earth Science, Tohoku University, 6-3, Aramaki Aza-Aoba, Aoba-ku, Sendai 980-8578, Japan

³Institute of Geoscience, Johannes Gutenberg University, Johann-Joachim-Becher-Weg 21, 55128 Mainz, Germany

Correspondence: Philipp Eichheimer (Philipp.Eichheimer@uni-bayreuth.de)

Abstract. Fluid flow on different scales is of interest for several Earth science disciplines like petrophysics, hydrogeology and volcanology. To parameterize fluid flow in large-scale numerical simulations (e.g. groundwater and volcanic systems), flow properties on the microscale need to be considered. For this purpose experimental and numerical investigations of flow through porous media over a wide range of porosities are necessary. In the present study we sinter glass bead media with various porosities and measure the permeability experimentally. The microstructure, namely effective porosity and effective specific surface, is investigated using image processing. We determine flow properties like ~~hydraulic~~ tortuosity and permeability using ~~both experimental measurements and~~ numerical simulations. ~~By fitting microstructural and flow properties to porosity, we obtain a modified Kozeny-Carman equation for isotropic low porosity media, that can be used to simulate permeability in large-scale numerical models. To verify the modified Kozeny-Carman equation we compare it to the computed and measured permeability~~ We test different parameterizations for isotropic low porosity media on their potential to predict permeability by comparing their estimations to computed and experimentally measured values.

1 Introduction

The understanding of transport and storage of geological fluids in sediments, crust and mantle is of major importance for several Earth science disciplines including volcanology, hydrology and petroleum geoscience (~~Manwart et al., 2002; Ramandi et al., 2017; Honarp~~ In volcanic settings melt segregation from partially molten rocks controls the magma chemistry, and outgassing of magmas influences both magma ascent and eruption explosivity (Collinson and Neuberg, 2012; Lamur et al., 2017; Mueller et al., 2005). In hydrogeology fluid flow affects ground water exploitation and protection (Domenico and Schwartz, 1998; Hölting and Coldewey, 2019), whereas in petroleum geoscience ~~fluid flow~~ it controls oil recovery efficiency (Suleimanov et al., 2011; Hendraningrat et al., 2013; Zhang et al., 2014).

A key parameter for fluid flow is permeability. Permeability estimations have been performed on several scales ranging from pore scale (Brace, 1980) to macroscale (~~Fehn and Cathles, 1979; Norton and Taylor Jr, 1979~~) (Fehn and Cathles, 1979; Norton and Taylor J As the permeability on the macroscale is a function of its microstructure it is necessary to accurately predict permeability based

on microscale properties (Mostaghimi et al., 2013). To achieve this goal, various experimental and numerical approaches have been developed over the years (e.g. Keehm, 2003; Andrä et al., 2013a; Gerke et al., 2018; Saxena et al., 2017).

25 Assuming laminar flow (Bear, 1988; Matyka et al., 2008), flow through porous media can be described using Darcy's law (Darcy, 1856), which relates the fluid flux Q to an applied pressure gradient-difference ΔP

$$Q = -\frac{k}{\eta} \frac{\Delta P}{L} \frac{kA\Delta P}{\eta L}, \quad (1)$$

where k is the permeability ~~and~~, A is the cross sectional area, η is the fluid viscosity ~~and~~ L is the length of the domain.

30 Accurately determining and predicting permeability is thus of crucial importance to quantify fluid fluxes in porous media. Until today it remains challenging to relate permeability to the microstructure of porous media. This has resulted in numerous parameterizations developed for different materials and structures (Kozeny, 1927; Carman, 1937, 1956; Martys et al., 1994; Revil and Cath

A first simple capillary model ~~for-to predict~~ the permeability of a porous ~~media-medium~~ was proposed by Kozeny (1927)

$$k = k_0 \frac{\phi^3}{S^2}, \quad (2)$$

where k_0 is the dimensionless Kozeny constant depending on the channel geometry (e.g. $k_0 = 0.5$ for cylindrical capillaries), ϕ is the porosity and S is the specific surface area (ratio of exposed surface area to bulk volume). Later this relation was extended by Carman (1937, 1956), ~~investigating the-to predict~~ fluid flow through a granular bed ~~,taking-its-microstructure-into-account.~~ ~~For-this-purpose-with-a-given-microstructure.~~ ~~To-account-for-the-effect-of-the-microstructure-on-fluid-flow,~~ Carman (1937, 1956) introduced the term tortuosity, ~~being-which-he-defined-as~~ the ratio of effective flow path L_e to a straight path L .

$$\tau = \frac{L_e}{L} \quad (3)$$

40 Introducing this relation into eq.(2) leads to the well-known Kozeny-Carman equation:

$$k = k_0 \frac{\phi^3}{\tau^2 S^2}, \quad (4)$$

Using experimental data, Carman (1956) determined that tortuosity τ is $\approx \sqrt{2}$. Today, the Kozeny-Carman equation - or variants thereof - is widely used in volcanology (Klug and Cashman, 1996; Mueller et al., 2005; Miller et al., 2014), hydrogeology (Wang et al., 2017; Taheri et al., 2017), two-/multi-phase flow studies (Wu et al., 2012; Keller and Katz, 2016; Keller and Suckale, 2019) a
45 soil sciences (Chapuis and Aubertin, 2003; Ren et al., 2016). The Kozeny-Carman equation was derived assuming that the medium consists only of continuous ~~,curved~~ channels with constant cross-section (Carman, 1937; Bear, 1988). However, in porous media pathways most likely do not obey these assumptions ~~and therefore applying~~. Applying this equation to porous media therefore remains challenging and in some cases fails for low porosities (Bernabe et al., 1982; Bourbie et al., 1992) or mixtures of different shapes and material sizes (Carman, 1937; Wyllie and Gregory, 1955). ~~This-has-led-to-modifications~~
50 ~~and-extensions-of-the~~ Consequently, alternative permeability parameterizations have been developed by different authors (Martys et al., 1994; Revil and Cathles III, 1999; Garcia et al., 2009).

Using numerical modeling, Martys et al. (1994) derived a universal scaling law for various overlapping and non-overlapping sphere packings which reads as:

$$k = \frac{2(1 - \phi - \phi_c)}{S^2} (\phi - \phi_c)^f, \quad (5)$$

55 with $f = 4.2$ and ϕ_c being the critical porosity, below which no connected pore space exists. They showed that eq.(5) is valid for a variety of porous media including mono-sized sphere packings, glass bead samples and experimentally measured sandstones. Despite the predictive power of this parameterization it might not give reasonable estimations for permeability in case the porous medium consists of rough surfaces and large isolated regions (voids).

The study of Revil and Cathles III (1999) used electrical parameters to derive the permeability of different types of shaly
60 sands, i.e., the permeability of a clay-free sand and the permeability of a pure shale. By using electrical parameters which separate pore throat from total porosity and effective from total hydraulic radius, Revil and Cathles III (1999) were able to improve the Kozeny-Carman equation and its parameters. For instance Mavko and Nur (1997) extended the Kozeny-Carman equation by considering a percolation threshold porosity ϕ_c , below which no continuous pathways exist. Additional modifications have been made to account for correlations between tortuosity, relation, being only dependent on grain size. In a first step the
65 authors developed a model for the permeability of a clay-free sand as a function of the grain diameter, the porosity, and the electrical cementation exponent reading as:

$$\Lambda = \frac{R^2}{2m^2 F^3}, \quad (6)$$

with Λ being the effective electrical pore radius, R being the grain radius, m being the cementation exponent and F being the formation factor. Using the relation of the formation factor to porosity by Archie's law $F = \phi^{-m}$ (Waxman and Smits, 1968),
70 $m = 1.8$ (Waxman and Smits, 1968) and $d = 2R$ for the grain diameter the authors derived a permeability parameterization for natural sandstones:

$$k = \frac{d^2 \phi^{5.1}}{24}, \quad (7)$$

which is in good agreement with experimentally measured data by Berg (1975).

Based on numerical simulations of fluid flow in polydisperse grain packings with irregular shapes, Garcia et al. (2009) proposed
75 an alternative parameterization by fitting the numerical results with the following equation:

$$k = \phi^{0.11} D^2, \quad (8)$$

where D^2 is the squared harmonic mean diameter of the grains. They also showed that this parameterization also fits experimental results quite well and concluded that grain shape and size polydispersity have a small but noticeable effect on permeability.

As can be seen from eq.(4),(5),(7),(8) the different parameterizations focus on specific types of porous media and relate
80 different microstructural properties to permeability. While properties such as porosity and mean grain diameter are relatively

straightforward to determine, others, such as specific surface and porosity-tortuosity, are much harder to access. This is why several parameterizations have been developed to quantify these properties (Comiti and Renaud, 1989; Pech, 1984; Mota et al., 2001; Pape et al., 2005). These studies either use experimental, analytical or numerical approaches for mostly two dimensional porous media with porosities $> 30\%$. Here, we fit correlations for three dimensional nearly isotropic spherical media in the low porosity regime ($< 22\%$), which can be compared to sandstones.

Since the ascent of Digital Rock Physics (DRP), it has become viable to study microstructures of porous media in more detail using micro Computed Tomography (micro-CT) and Nuclear Magnetic Resonance (NMR) images (Arns et al., 2001; Arns, 2004; Dvorkin et al., 2011). Using these images it is possible. Together with numerical models, these images can then be used to compute fluid flow and several microstructural properties like porosity and specific surface as well as fluid properties including tortuosity and within porous media to determine their permeability. For this purpose several numerical methods including Finite Elements (FEM), Finite Differences (FDM) and Lattice Boltzmann method (LBM) (Saxena et al., 2017; Andrä et al., 2013a; Gerke et al., 2018; Shabro et al., 2014; Manwart et al., 2002; Bird et al., 2014) can be have been used.

Parameterizing those microstructural and fluid flow properties, which can be used as input for large-scale numerical models requires systematic data sets. Yet, very few data sets exist that systematically investigate microstructure (porosity and specific surface) and related flow parameters (tortuosity and permeability) using systematically sintered samples $< 22\%$ porosity, in particular at porosities $< 30\%$. Most of the previous studies either measure permeability experimentally without investigating its microstructure or compute permeability and related microstructural parameters, but can not compare that cannot be compared to experimental data sets as structural images are not available. For this reason we sinter isotropic. To remedy this issue, we here sinter porous glass bead samples with porosities ranging from $1.5\% - 22\%$, representing $1.5\% - 21\%$ and investigate their microstructure using image processing. This porosity range is representative of sedimentary rocks up to a depth of ≈ 20 km (Bekins and Dreiss, 1992). The microstructure is investigated using image processing. Permeability is Permeability is then measured experimentally using a permeameter (see sec.2.2; Takeuchi et al. (2008); Okumura et al. (2009)) and numerically using the finite difference code LaMEM (see sec.2.7; Kaus et al. (2016); Eichheimer et al. (2019)). Theoretical permeability predictions (eq.(4)) require three input parameters, namely The theoretical permeability predictions described above in eqs.(4),(5),(7),(8) require microstructural input parameters such as porosity, specific surface and hydraulic tortuosity. Within this study these parameters are determined and related to the porosity. Thus, we are able to provide a modified Kozeny-Carman equation porosity. We therefore provide permeability parameterizations depending on porosity only and verify against numerically and experimentally determined values.

2 Methods

Here we first describe the experimental workflow including sample sintering and permeability measurement, followed by the numerical workflow featuring image processing, computation of fluid velocities and determination of both hydraulic tortuosity and permeability. Fig.1 shows an overview of the entire workflow which will be explained in detail in the following section.

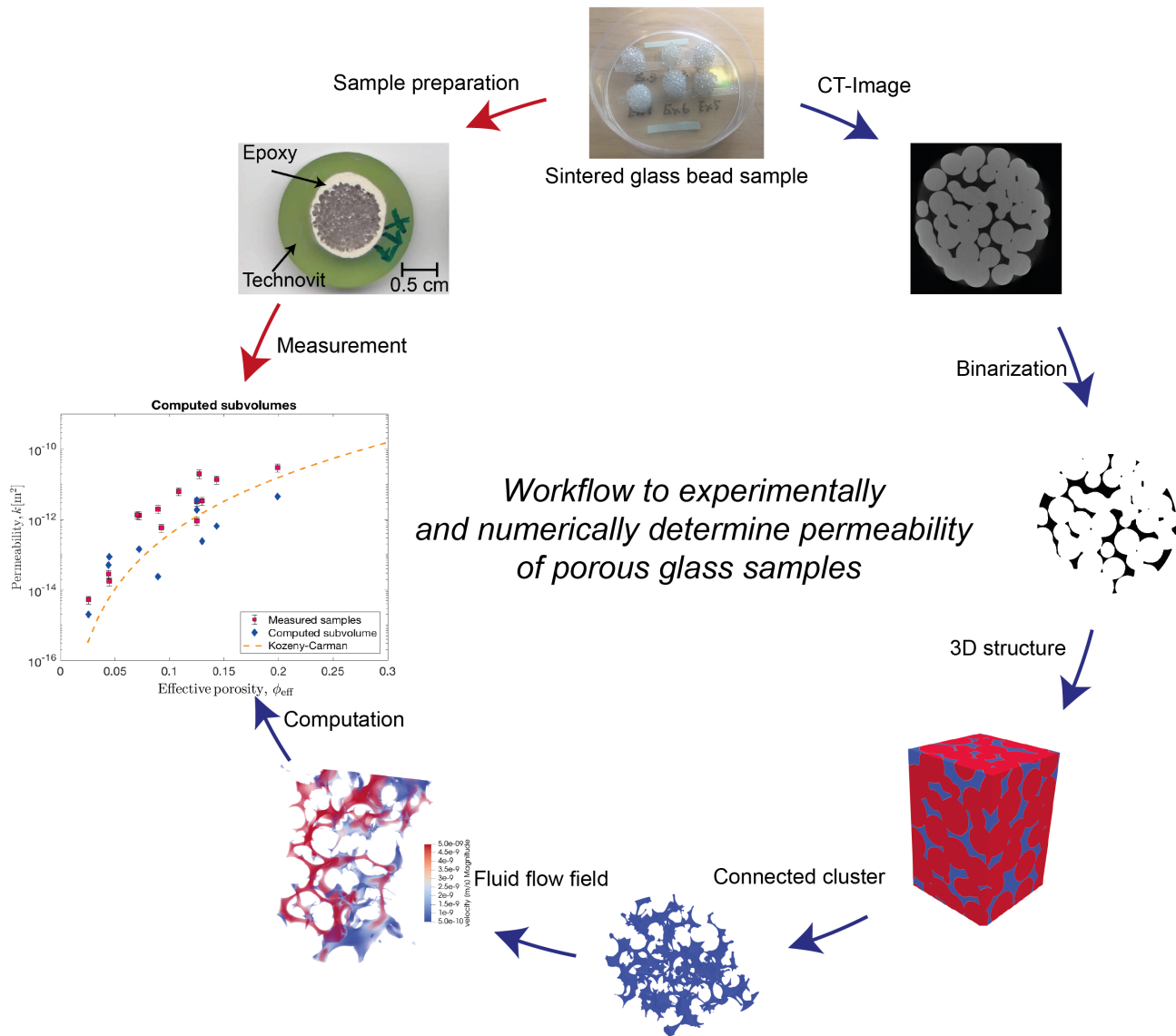


Figure 1. Workflow process map - red arrows mark the experimental workflow, whereas blue arrows indicate the numerical workflow.

2.1 Sample sintering

115 Glass bead cylinders with different porosities were sintered under experimental conditions as summarized in Table 1. For this purpose soda-lime glass beads with diameters ranging from 0.9 to 1.4 mm were utilized as starting material (see grain size distribution in [see:appendix D](#)). For each sample, we prepared a graphite cylinder with 8.0 mm inner diameter and ≈ 10 mm height. Additional samples with diameters of 10 and 14 mm were prepared to check for size effects (see [tab.1a](#)). At the bottom

of the graphite cylinder a graphite disc (11.5 mm diameter and 3.0 mm thick) was attached using a cyanoacrylate adhesive (see fig.2 inset). The glass beads were poured into the graphite cylinder and compressed with steel rods (8-14 mm diameter) before heating.

The glass bead samples were then sintered in a muffle furnace at 710°C under atmospheric pressure. The temperature of 710°C was found to be suitable for sintering of the glass beads as it is slightly below the softening temperature of soda-lime glass around 720 – 730°C (Napolitano and Hawkins, 1964) and well above the glass transition temperature of soda-lime glass at ≈550°C (Wadsworth et al., 2014). At 710°C the viscosity of the employed soda-lime glass is on the order of 10^7 Pa·s (Kuczynski, 1949; Napolitano and Hawkins, 1964; Wadsworth et al., 2014) allowing for viscous flow of the glass beads at their contact surface driven by surface tension. Using different time spans ranging from 60 – 600 minutes the viscous flow at 710°C controls the resulting porosity of the sample.

After sintering, the sample was cooled down to 550 – 600°C within ≈5 minutes. Afterwards the sample was taken out of the furnace to adjust to room temperature ~~to~~ and prevent thermal cracking of the sample. In a next step the graphite container was removed from the sample. It should be noted that during the process of sintering gravity slightly affects the porosity distribution within the glass bead sample (see fig.2). However, the subsamples used to compute the numerical permeability do not cover the whole height of the sample, thus the effect of compaction on the results is limited.

2.2 Experimental permeability measurement

In a first preparation step we wrap a highly viscous commercial water resistant resin around the sample to avoid pore space infiltration. In a next step we embed the sample within a less viscous resin (Technovit 4071, Heraeus Kulzer GmbH & Co. or Presin, Nichika Inc.) to create an airproof casing. The upper and lower surface of the sample were grinded and polished to prevent leaks during experimental permeability measurements (fig.1; Sample preparation).

The experimental permeability measurements were conducted at Tohoku University using a permeameter, described in Takeuchi et al. (2008) and Okumura et al. (2009). To determine the permeability the air flow through a sample is measured at room temperature. The pressure gradient between sample inlet and outlet is controlled by a pressure regulator (RP1000-8-04, CKD Co.; Precision ±0.1%) at the inlet side. To monitor the pressure difference a digital manometer (testo526-s, Testo Inc.; Precision ±0.05%) is used. Air flow through the sample is measured using a digital flow meter (Alicat, M-10SCCM; Precision ±0.6%). As Darcy's law assumes a linear relationship between the pressure and flow rate, we measure the gas flow rate at several pressure gradients (see fig.C1 in Appendix AC) to verify our assumption of laminar flow conditions. The permeability of all samples is calculated using Darcy's law (eq.(1)) ~~;~~ ~~the measured values and additional parameters (Tab.1~~ based on measured values (tab.1a).

2.3 Micro-CT images and segmentation

Before preparing the samples for permeability measurements all samples are digitized using micro Computed Tomographic scans (micro-CT) performed at Tohoku University (ScanXmate-D180RSS270) with a resolution ≈ 6 – 10 μm according to the method of Okumura and Sasaki (2014). Andrä et al. (2013b) showed that the process of segmentation of the micro-CT images

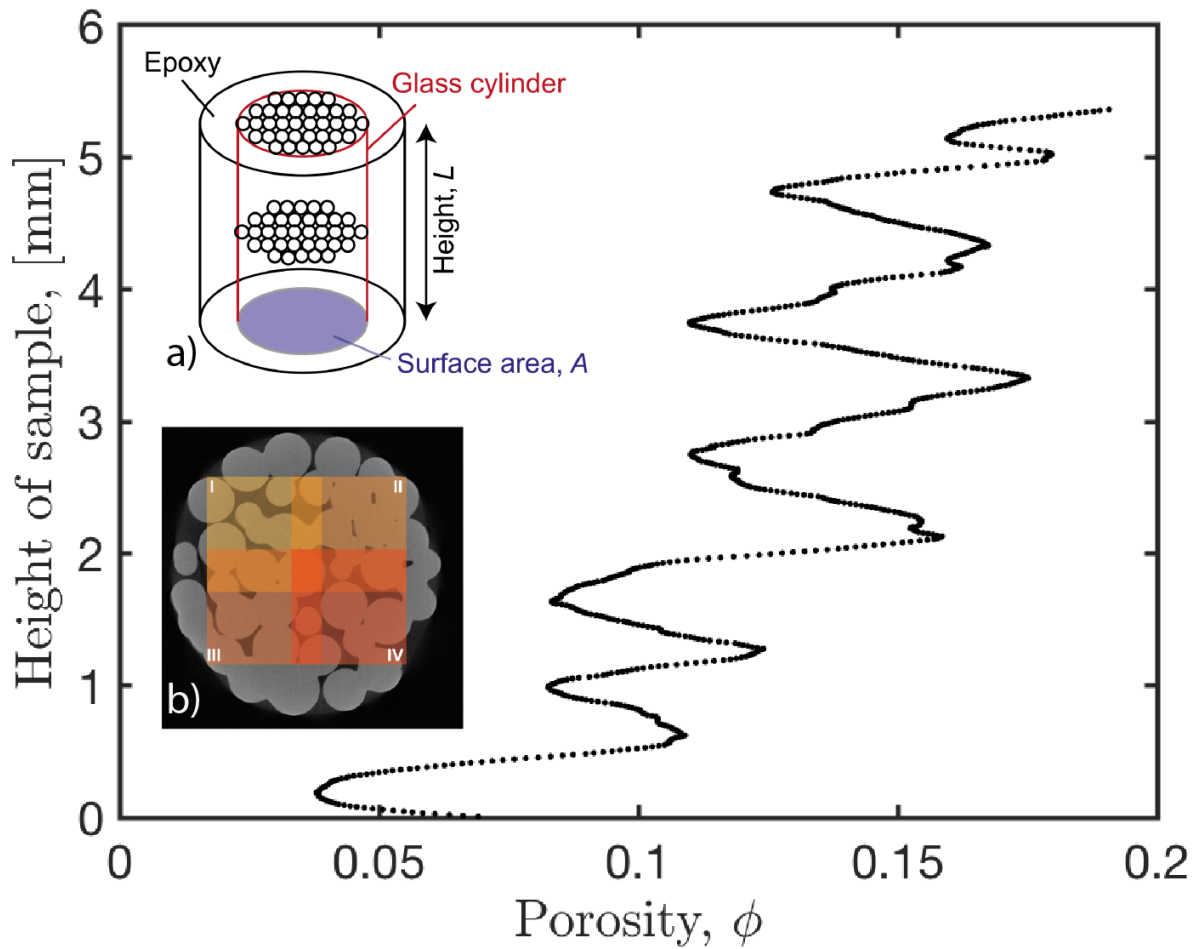


Figure 2. Computed porosity of each CT-slice from top to the bottom of a full sample (z-axis; sample Ex14). The diagram shows that gravity affects the porosity of the sample. Porosity minima correspond to distinct layers of glass bead within the sample. The inset **a)** provides a sketch of the sample structure. In the inset the red color outlines the cylindrical shape, blue the surface area A of the cylinder and L the height of the sample. **b)** shows chosen locations for the squared subsamples 1-4. Additional four subsamples (5-8) are placed similarly below subsamples 1-4 overlapping in z-direction.

may have a significant effect on the three dimensional pore space and therefore the computed flow field. In two-phase systems (fluid + mineral), as in this study, the segmentation is straightforward due to the high contrast in absorption coefficients between glass beads and air, while it can become quite complex for multiphase systems featuring several mineral phases. In the present study the segmentation of the obtained micro-CT images was done using build-in MatLab functions. In a first step the images are binarized using Otsu's method (Otsu, 1979). Additional smoothing steps of the images are performed. In a next step the

Table 1. Experimental a) displays experimental parameters of sintering conditions and parameters used to compute permeability using Darcy’s law. A denotes the sample surface area, L the height of the glass bead cylinders and D the inner diameter of each capsule. The Additionally, the sintering time in minutes t_{sint} , the total weight of the glass beads m , and the experimentally measured permeability K_{meas} are given. The In b), we list the total, effective and minimum effective porosity ϕ_{tot} , ϕ_{eff} shown here is computed using, $\min(\phi_{\text{eff}})$ of each sample. These porosities have been obtained with image processing (see sec. 2.4).

Sample	a) Experimental parameters						b) Numerical parameters			
Sample	Area A (% cm^2)	Height L (% mm)	Capsule \emptyset D (% mm)	Time t_{sint} (cm^2min)	Tot. weight m (mmg)	Permeability K_{meas} (mm^2)	Porosity ϕ_{tot} ($\text{min}\%$)	Porosity ϕ_{eff} ($\text{g}\%$)	m	
X02	20.94 20.94	0.438	5.11	8	120	0.574	$(3.1 \pm 0.2) \times 10^{-11}$	X11	6.72 20.94	4.75 20.94
X11	0.434	3.63	8	180	0.575	$(1.91 \pm 0.09) \times 10^{-14}$	X14	13.28 6.72	13.22 4.75	
X14	0.407	5.12	8	60	0.576	$(3.4 \pm 0.2) \times 10^{-12}$	X15	2.54 13.28	1.21 13.22	
X15	0.412	4.76	8	480	0.575	$(5.7 \pm 0.3) \times 10^{-15}$	X16	6.07 2.54	4.50 1.21	
X16	0.808	5.05	10	120	0.899	$(3.1 \pm 0.2) \times 10^{-14}$	X17	12.90 6.07	12.85 4.50	
X17	1.569	5.18	14	120	1.762	$(1.41 \pm 0.07) \times 10^{-12}$	X29	9.01 12.90	8.97 12.85	
X29	0.441	4.55	8	300	0.576	$(6.3 \pm 0.3) \times 10^{-13}$	X30	7.12 9.01	7.03 8.97	
X30	0.420	4.81	8	600	0.574	$(1.52 \pm 0.08) \times 10^{-12}$	X31	9.92 7.12	9.87 7.03	
X31	0.423	4.73	8	300	0.576	$(2.1 \pm 0.1) \times 10^{-12}$	X32	13.52 9.92	13.44 9.87	
X32	0.342	4.47	8	480	0.576	$(3.7 \pm 0.2) \times 10^{-12}$	X33	15.97 13.52	15.96 13.44	
X33	0.412	4.80	8	180	0.575	$(1.53 \pm 0.08) \times 10^{-11}$	X35	14.17 15.97	14.15 15.96	
X35	0.411	4.78	8	360	0.575	$(2.2 \pm 0.1) \times 10^{-11}$	X36	10.71 14.17	10.67 14.15	
X36	0.372	4.15	8	420	0.575	$(6.9 \pm 0.4) \times 10^{-12}$		10.71	10.67	

two dimensional micro-CT slices are stacked on top of each other, resulting in a three dimensional representation of the pore space (fig.1; 3D structure). As isolated clusters of

2.4 Porosity determination

Porosity is an important parameter describing microstructures. It is defined as the ratio of the total pore space V_V to the bulk volume of the sample V_b (Bird et al., 2006):

$$\phi_{\text{tot}} = \frac{V_V}{V_b} \quad (9)$$

In a first step, the total porosity of each sample is determined by counting the amount of solid and fluid voxels. In a second step, we determine the isolated pore space do not contribute to the permeability, we extract all percolating clusters of pore space using a flooding algorithm implemented in MatLab (bwconncomp). This isolated pore space is then subtracted from the total pore space to obtain an effective pore space V_{eff} . As a bonus, this procedure reduces the computational cost for numerical

permeability determinations by removing irrelevant the parts of the pore space -that do not contribute to fluid flow and thus permeability. The effective porosity ϕ_{eff} is then defined as the volume of all percolating pore space clusters $V_{V_{\text{eff}}}$ to the bulk volume of the sample:

$$\phi_{\text{eff}} = \frac{V_{V_{\text{eff}}}}{V_b} \quad (10)$$

170 It should be mentioned that in a simple capillary model $\phi_{\text{eff}} = \phi$ since no isolated pore space exists. It should also be noted that only the effective porosity is used to determine microstructural and flow properties later in this study.

As described in section 2.1, the porosity of the samples is not homogeneous, but increases towards the sample bottom due to gravity. As permeability may not necessarily be affected by the total porosity, but rather by the minimum effective porosity in a sample (in a slice perpendicular to the flow direction), we also determined the minimum effective porosity of each sample (see tab.1b).

2.5 Effective specific surface

The specific surface is defined as the total interfacial surface area of pores A_s per unit bulk volume V_b of the porous medium (Bear, 1988):

$$S = \frac{A_s}{V_b} \quad (11)$$

180 As in the previous section we compute the effective specific surface of all percolating pore space clusters and neglect isolated pore space. To determine the effective specific surface we use the extracted connected clusters and compute an isosurface of the entire three dimensional binary matrix. In a next step the area of the resulting isosurface A_s is calculated.

2.6 Numerical method

The relationship between inertial and viscous forces in fluid flows is described by the Reynolds number:

$$185 \quad Re = \frac{\rho v L}{\eta}, \quad (12)$$

where ρ is the density, v the velocity component, L denotes the length of the domain and η is the viscosity of the fluid. For laminar flow conditions ($Re < 1$, see fig.C1 Appendix A C) and ignoring gravity, the flow in porous media can be described with the incompressible Stokes equations:

$$\frac{\partial v_i}{\partial x_i} = 0 \quad (13)$$

$$190 \quad \frac{\partial}{\partial x_j} \left[\eta \left(\frac{\partial v_i}{\partial x_j} + \frac{\partial v_j}{\partial x_i} \right) \right] - \frac{\partial P}{\partial x_i} = 0 \quad (14)$$

with P being the pressure and x the spatial coordinate. For all simulations, we employed a fluid viscosity of 1 Pa-s Pas.

The Stokes equations are solved using the finite difference code LaMEM (Kaus et al., 2016; Eichheimer et al., 2019). LaMEM employs a staggered grid Finite Difference scheme (Harlow and Welch, 1965), where pressures P are defined at the cell centers and velocities v at cell faces. Based on the data from the CT-scans, each cell is assigned either a fluid or a solid phase. The discretized system of equations is then solved using multigrid solvers of the PETSc library (Balay et al., 2019). As only cells within the fluid phase contribute to fluid flow the discretized governing equations are only solved for these cells. This greatly decreases the number of degrees of freedom and therefore significantly reduces the computational cost. Due to computational limitations and the densification at the bottom of the samples (see fig.2) we extract 8 overlapping subvolumes per full sample (see fig.2b), with sizes of 512^3 cells. For each subvolume we compute effective porosity, effective specific surface, hydraulic tortuosity and permeability.

2.7 Numerical permeability computation

From the calculated velocity field in z -direction the volume-averaged velocity component v_m is calculated (e.g. Osorno et al., 2015):

$$v_m = \frac{1}{V_f} \int_{V_f} |v_z| dv, \quad (15)$$

where V_f is the volume of the fluid phase. Using Darcy's law (eq.1; Andrä et al., 2013a; Bosl et al., 1998; Morais et al., 2009; Saxena et al., 2017) an intrinsic permeability k_s is computed via:

$$k_s = \frac{\eta v_m}{\Delta P} \quad (16)$$

2.8 ~~Effective porosity~~Hydraulic tortuosity

~~Porosity is an important parameter describing microstructures. It is defined as the ratio of pore space V_V to the bulk volume of the sample V_B (Bird et al., 2006):-~~

$$\phi = \frac{V_V}{V_B}$$

~~In Tortuosity is not only highly relevant for the Kozeny-Carman relation, but is also used in various engineering and science applications (Nemati et al., 2020). It has a major influence on liquid-phase mass transport (e.g. in Li-ion batteries (Thorat et al., 2009) and membranes (Manickam et al., 2014)), the effectiveness of tertiary oil recovery (Azar et al., 2008) and evaporation of water in soils (Hernández-López et al., 2014). In recent years, several definitions for tortuosity have been suggested (Clennell, 1997; Bear, 1988; Gh~~
~~For the remainder of this study we compute an effective porosity for each sample from its obtained micro-CT data. In our case the effective porosity is defined as the porosity of all percolating clusters of pore space to the total volume of material:-~~

$$\phi_{eff} = \frac{V_{V_{eff}}}{V_B}$$

~~will calculate and apply the so-called hydraulic tortuosity (Ghanbarian et al., 2013). Assuming that hydraulic tortuosity changes with porosity, both numerical and experimental studies published different relations of hydraulic tortuosity to porosity. In most~~

of the cases the hydraulic tortuosity is assumed to be constant as it is difficult to determine experimentally, which is rarely done. It should be mentioned that in a simple capillary model $\phi_{\text{eff}} = \phi$ since no isolated pore space exists. Further it should be noted that we only use the effective porosity to determine microstructural and flow parameters.

2.9 Effective specific surface

225 The specific surface is defined as the total interfacial surface area of pores A_s per unit bulk volume V_b of the porous medium (Bear, 1988):

$$S = \frac{A_s}{V_b}$$

As in the previous section we compute the effective specific surface of all percolating clusters of pore space and neglect isolated pore space.

230 2.9 Hydraulic tortuosity

In recent years several definitions for hydraulic tortuosity have been suggested (Clennell, 1997; Bear, 1988; Ghanbarian et al., 2013). Numerically Matyka et al. (2008) the following hydraulic tortuosity-porosity relations have been obtained for porous media with $> 30\%$ porosity.

Matyka et al. (2008) numerically determined the hydraulic tortuosity by using an arithmetic mean given as:

$$235 \quad \tau_h = \frac{1}{N} \sum_{i=1}^N \tau(r_i), \quad (17)$$

where $\tau = L_e/L$ is the hydraulic tortuosity of a flow line crossing through point r_i (eq.(3)) and N the total number of streamlines.

Koponen et al. (1996) computed the hydraulic tortuosity numerically using:

$$\tau_h = \frac{\sum_i \tau^n(r_i) v(r_i)}{\sum_i v(r_i)}, \quad (18)$$

240 where $v(r_i) = |v(r_i)|$ is the fluid velocity at point r_i and points r_i are chosen randomly from the pore space (Koponen et al., 1996).

Both numerical and experimental studies published different relations of hydraulic tortuosity to porosity. One of the most common relations for hydraulic tortuosity is a logarithmic function of porosity reading as follows:

$$\tau_h(\phi) = 1 - B \ln(\phi), \quad (19)$$

245 where B is a constant found experimentally for different particles (e.g. 1.6 for wood chips Pech (1984); Comiti and Renaud (1989) (Pech, 1984) 0.86 to 3.2 for plates Comiti and Renaud (1989) (Comiti and Renaud, 1989)). By numerically computing hydraulic tortuosity for two dimensional squares, Matyka et al. (2008) obtained $B = 0.77$. A different experimental relation for hydraulic tortuosity

measuring the electric conductivity of spherical particles was proposed by Mota et al. (2001):

$$\tau_h(\phi) = \phi^{-0.4} \quad (20)$$

250 Investigating numerically two-dimensional porous media with rectangular shaped particles Koponen et al. (1996) proposed a different relation:

$$\tau_h(\phi) = 1 + 0.8(1 - \phi) \quad (21)$$

~~It should be mentioned that the tortuosity-porosity relations stated above mostly have been obtained for porous media with $\geq 30\%$ porosity. In the present study the hydraulic tortuosity is determined according to eq.(17). To compute the hydraulic~~
255 ~~tortuosity pathways, which requires to compute the tortuosity τ for each sample need to be computed. Pathways of individual streamlines within each sample. Streamlines~~ describe a curve traced out in time by a fluid particle with fixed mass and ~~reads~~
~~mathematically as~~ are described mathematically as:

$$\frac{\partial x_i}{\partial t} = v(x, t), \quad (22)$$

with v being the computed velocity field obtained from the numerical simulation and t being the time. Integrating eq.(22)
260 yields

$$x_i = x_i(x^0, t), \quad (23)$$

where x^0 is the position of the prescribed particle at $t = 0$. Eq.(22)-(22) is solved using built-in MatLab ODE (Ordinary Differential Equation) solvers. To compute the ~~pathway-streamline~~ length all fluid cells at the inlet of the subsample are extracted and used as streamline starting points. Using the computed velocity field and eq.(22) the ~~pathway-streamline~~ length
265 for each ~~extracted fluid cell starting point~~ is calculated. Hence, up to 40000 ~~pathways-needs streamlines need~~ to be computed for a ~~subsamples-subsample~~ with $\approx 20\%$ porosity, whereas for a ~~subsamples-subsample~~ with $\approx 5\%$ porosity up to 5000 ~~pathways streamlines~~ are computed. ~~The resulting length of each pathway is used to compute the hydraulic tortuosity according to eq.(17).~~

3 Results

270 In this section we ~~present results on microstructural properties like effective specific surface and flow properties like~~ analyze the different samples in terms of porosity, specific surface, hydraulic tortuosity and permeability. All data for each subsample presented here are given in the supplementary tables (see table 1 - 13). Effective porosity and effective specific surface are computed for both subsamples and full samples, whereas hydraulic tortuosities and ~~permeability permeabilities~~ are only computed for ~~the~~ subsamples due to computational limitations. In the present study we analysed 13 samples and 104 subsamples.

275

3.1 Porosity

The total porosity for each sample and subsample is analysed using image processing and ranges from 2.5 – 21% (see tab. 1b and supplement table 1-13). The effective porosity is determined by extracting all connected clusters within the samples and ranges from 1.21 – 21% (see also tab.1b). The analysis of the micro CT images also showed that during sintering densification of the samples occurs (see fig.2). For this reason we furthermore report the minimum effective porosity $\min(\phi_{\text{eff}})$. Assuming an effective porosity for the entire sample therefore does not seem to be representative as during the laboratory measurements a first order control mechanism of the fluid flow and therefore permeability is the lowest porosity within the entire sample.

3.2 Effective specific surface

Figure 3 shows the computed specific surfaces for all subsamples and all full samples with increasing effective porosity. Koponen et al. (1997) used the following relationship to predict the specific surface:

$$S = -\frac{n}{R_0} \phi_{\text{eff}} \ln(\phi_{\text{eff}}), \quad (24)$$

where n is the dimensionality and R_0 is the hydraulic radius of the particles. The hydraulic radius is defined as $2V_p/M$ (e.g. Bernabé et al., 2010), with V_p being the pore volume and M being the pore surface area. For a regular simple cubic sphere packing with $\phi = 0.476$ the estimated hydraulic radius is $\approx 151 \mu\text{m}$. To relate the computed values for the effective specific surface to the effective porosity the above equation is fitted, resulting in a hydraulic radius of $385.09 \mu\text{m}$.

$$S = -\frac{3}{3.8509 \times 10^{-4} \text{ m}} \phi_{\text{eff}} \ln(\phi_{\text{eff}}) \quad (25)$$

The fit between eq.(24) and our data shows good agreement expressed in terms of the R^2 parameter, representing to which extent a fit represents the data points, equal to ≈ 0.975 (see fig.3). Thus our fit of effective specific surface to effective porosity reads as follows:-

$$S(\phi_{\text{eff}}) = -\frac{3}{3.8509 \times 10^{-4} \text{ m}} \phi_{\text{eff}} \ln(\phi_{\text{eff}})$$

3.3 Hydraulic tortuosity

Figure 4 compares We computed hydraulic tortuosities for all subsamples which exhibit a percolating pore space. Results are shown in fig. 4, where we compare different hydraulic tortuosity-porosity relations parameterizations presented in section 2.8 to our data. Figure In fig.4a) shows the published porosity-tortuosity relation from -c), we compare our data (denoted by grey squares) with one of the three porosity-hydraulic tortuosity parameterizations (denoted by solid and dashed lines), whereas in fig.4d), we show a simple linear fit to our data. In general, computed hydraulic tortuosities are quite scattered and show variations ranging from values of about 2 to values of around 4. In fig.4a) we compare our data to the hydraulic tortuosity parameterization from Matyka et al. (2008) (see eq.(19)) represented (19), which is denoted by a dashed black line. The

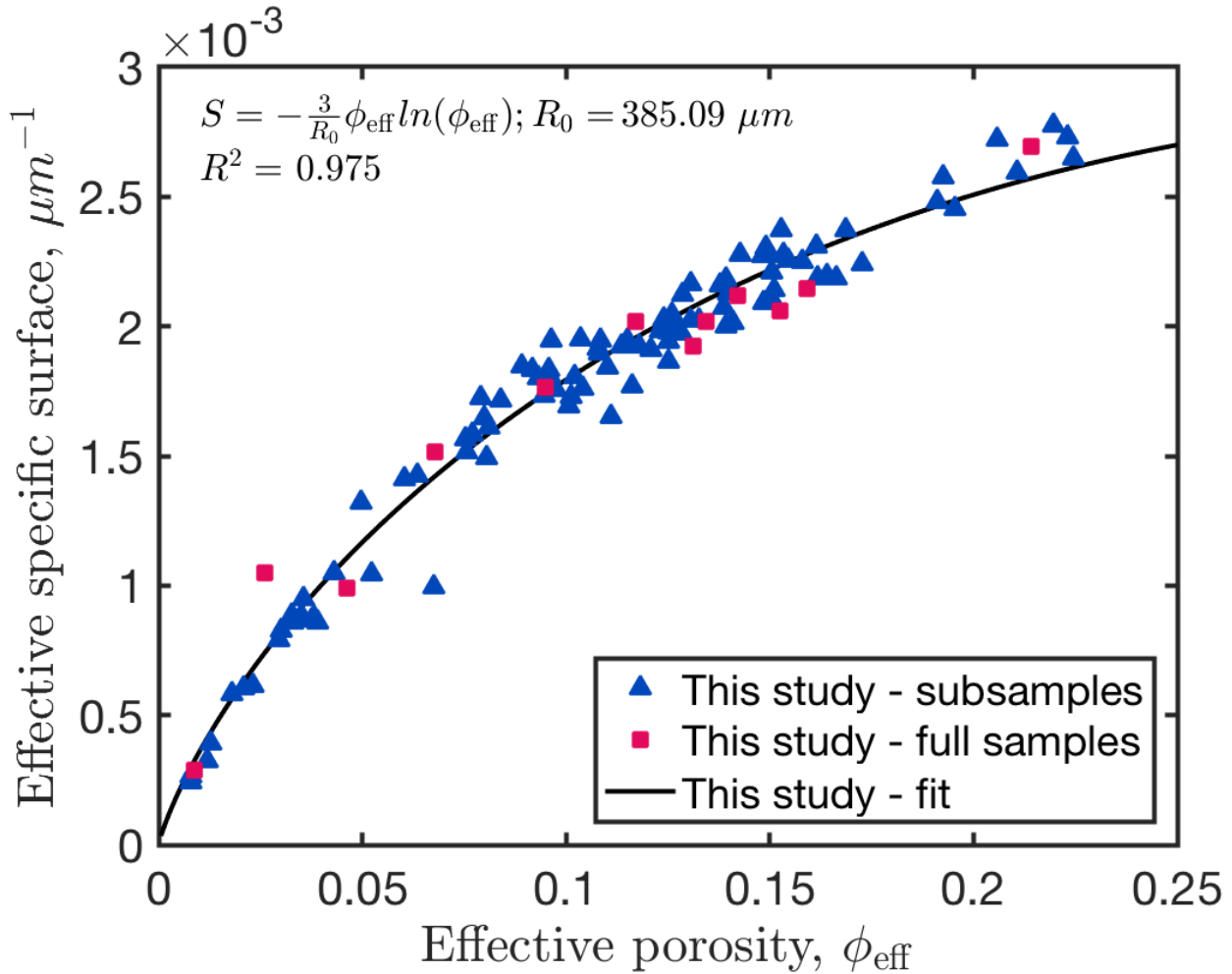


Figure 3. Effective specific surface as a function of effective porosity. Blue triangles represent subsample data from this study and red squares the effective specific surface of full samples. Full sample data points are plotted in order to show that in terms of effective specific surface subsamples represent full samples very well. The black curve represents the fitted curve according to eq.(25).

305 ~~fitted relation is given by a red~~ We refitted this parameterization using our data, with the result shown by the red solid line
with corresponding 95% confidence bounds ~~.Figure~~ with the coefficient of determination $R^2 = -1.6317$. In fig.4b) displays
~~the hydraulic tortuosity-porosity relations proposed and c), similar comparisons are shown, but for the parameterizations~~ by
Koponen et al. (1996) (see eq.(21)) ~~symbolized by the dashed black line and in yellow our fit to the computed hydraulic~~ tortuosity. Additionally figure ~~fig.4b) and Mota et al. (2001) (fig.4c)~~ presents the relation of Mota et al. (2001) (see eq. (20)). It
310 ~~should be noted that hydraulic tortuosities in figure 4a, c and d are computed according to eq. (17), whereas tortuosities in~~ figure 4b are computed using eq.(18). As can be seen in figure 4a-e our computed hydraulic tortuosities do not agree well with
~~the models suggested by previous studies. The~~ . In both cases, we show the original parameterizations as a black dashed line

and the fitted parameterizations as a colored solid line with colored dashed lines indicating the 95% confidence bounds. As for the parameterization by Matyka et al. (2008), these two parameterizations do not fit our data very well, as is also indicated by their low R^2 values for these fits are either negative or quite small, which shows that the arithmetic mean is an equivalent good fit. Apart from some scattering, our hydraulic tortuosity values appear to be almost constant independent of the effective porosity. The computed hydraulic tortuosities of the present study can be fitted using the following equation plotted in figure 4d:

$$\tau_h(\phi_{\text{eff}}) = -0.8712\phi_{\text{eff}} + 3.021$$

Yet ($R^2 = -5.6017$ and $R^2 = 0.0758$ respectively). Finally, in fig. 4c), we show a linear fit to our data together with the 95% confidence bounds. As indicated by the low R^2 value of 0.0274, this fit does not represent a good correlation, represented by a low R^2 value. We therefore use both also not represent the data very well. For this reason we use the arithmetic mean and eq. (??) for later theoretical of the computed hydraulic tortuosities for later permeability predictions. The relatively constant tortuosity, in contrast with many previous models in which tortuosity increases with porosity. Nevertheless, we do observe that despite the large scatter, hydraulic tortuosity largely remains relatively constant with decreasing porosity, shows thus indicating that the pore distribution of our experimental products is homogeneous and the geometrical similarity of pore structure was kept during sintering. This is in contrast to the parameterizations of Matyka et al. (2008) and Mota et al. (2001), both predicting a significant increase in tortuosity as small porosities are approached, but agrees with the model of Koponen et al. (1996).

3.4 Permeability prediction

To predict the permeability of the respective samples, the expressions for effective specific surface and hydraulic tortuosity are inserted into the Kozeny-Carman equation (eq. (4)):-

$$k = k_0 \frac{(\phi_{\text{eff}} - \phi_c)^3}{\tau(\phi_{\text{eff}})^2 S(\phi_{\text{eff}})^2}$$

with $k_0 = 0.5$ being the geometrical parameter for spherical particles (Kozeny, 1927) and $\phi_c = 0.015$ as the critical porosity threshold based on the lowest measured values. In fig. 5, measured permeabilities for all samples are shown as grey symbols (see also tab. 1a for measured values). We here chose to plot sample permeabilities vs. the minimum of the effective porosity, the reason being the intrinsic porosity variations in each sample (see section 2.4). Figure A1 in the appendix shows both the effective porosity and minimum effective porosity of a subsample from our study showing a continuous pathway. The critical porosity threshold ϕ_c in this study is lower than the value of $\phi_c = 0.03$ calculated by previous studies (Van der Marek, 1996; Rintoul, 2000; Wadsworth et al., 2016) is related to the formation of dead-ends during sintering (see Appendix ??) each sample.

Measured permeabilities range from values of around 10^{-14} m^2 to about 10^{-11} m^2 , depending on porosity. Although experimental measurements are scattered, a clear trend can be observed. At porosities close to the critical porosity, permeabilities are very low, but rapidly increase when porosities increase slightly. At larger porosities, permeabilities further increase, but this increase is significantly less rapid.

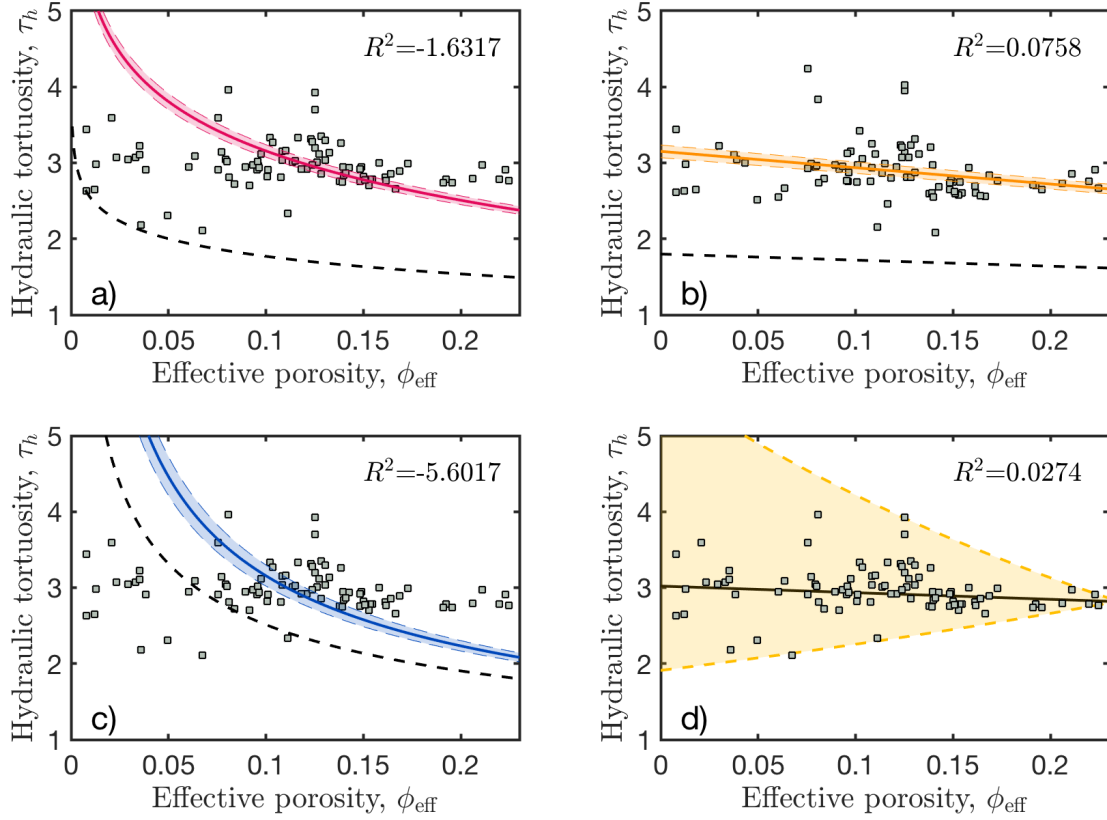


Figure 4. (a)-(c) show the proposed relations for the hydraulic tortuosity according to (a) Matyka et al. (2008), (b) Koponen et al. (1996) and (c) Mota et al. (2001) as black dashed lines. The colored solid lines represent the fit of the computed data to those relations within the 95% confidence bounds. Hydraulic tortuosities for all subsamples (grey squares) are computed according to the method used in each of these studies. (d) shows the fit [found-obtained](#) in the present study. The colored area in (d) illustrates the extending distribution of computed hydraulic tortuosities with decreasing effective porosity.

345 [Numerically 98 subsamples have been computed successfully with permeabilities ranging from around \$10^{-14} \text{ m}^2\$ to about \$10^{-10} \text{ m}^2\$, depending on porosity \(see table 1-13 in the supplement and fig.B1 in the appendix\). In comparison to the experimentally measured samples, the numerical permeabilities tend towards higher values, but show a clear trend.](#)

As ~~the fit for hydraulic tortuosity is not very good, we additionally use the arithmetic mean of all computed hydraulic tortuosities as input for eq. (??). Using eq. (??) the parameterization for permeability reads:-~~

$$k = k_0 \frac{(\phi_{\text{eff}} - \phi_c)^3}{[(-0.8712\phi_{\text{eff}}) + 3.021]^2 \cdot \left[-\frac{3}{3.8509 \times 10^{-4} \text{ m}} \phi_{\text{eff}} \ln(\phi_{\text{eff}})\right]^2},$$

350 ~~Furthermore only using the arithmetic mean the parameterization denotes:~~ we split each sample in eight subsamples for numerical permeability computations, we need to average them to compute an effective sample permeability that can then be compared to measured values. This upscaling issue is not trivial to address and it is not clear yet which averaging method is appropriate. It is possible to put bounds on the effective permeability by using either the arithmetic or harmonic mean of subsample permeabilities. However, these bounds correspond to very specific geometrical sample structures. In the case of the arithmetic mean, the medium is assumed to consist of parallel layers oriented parallel to the flow direction whereas the harmonic mean is valid in the case of parallel layers orthogonal to the flow direction. This is most often not the case. Therefore, different averaging methods have been developed to obtain adequate upscaling procedures for heterogeneous porous media (e.g. Sahimi, 2006; Jang et al., 2011; Torquato, 2013). One of the simplest averaging schemes that has been shown to be an appropriate approximation for heterogeneous porous media is the geometric mean (e.g. Warren and Price, 1961; Selvadurai and Selvadurai, 360 which reads as:

$$k_g = \left(\prod_{i=1}^n k_0 \frac{(\phi_{\text{eff}} - \phi_c)^3}{2.9715^2 \cdot \left[-\frac{3}{3.8509 \times 10^{-4} m} \phi_{\text{eff}} \ln(\phi_{\text{eff}}) \right]^2} \right)^{1/n} \quad (26)$$

To assess the predictive power of this parameterization, we compare the predictions made by eq.(??) and eq. (27) to both experimentally and numerically determined permeabilities (where i is the number of the subsample and n the total number of subsamples (eight in this study). As several subsamples at low porosities did not exhibit a connected pore space (thus not allowing for any fluid flow), we assumed a permeability of 10^{-20} m^2 for these samples. The geometric averages of each subsample set are shown in fig.5. 365

To determine the predictive power of the different permeability parameterizations described in section 1, we inserted the expressions for effective specific surface and hydraulic tortuosity into the respective equations (eq.(4) & (5)). The permeability estimation lies in between measured and computed values for permeability. While experimentally determined permeability values yield towards lower permeabilities, computed permeabilities tend to lie above the estimation obtained from the 370

The Kozeny-Carman equation. In particular, for very low porosities the computed values differ from the permeability prediction. Furthermore values for some computed subsamples are several orders of magnitude higher than the theoretical permeability predictions. As some then reads as:

$$k = k_0 \frac{[\min(\phi_{\text{eff}}) - \phi_c]^3}{2.9715^2 \cdot \left[-\frac{3}{3.8509 \times 10^{-4} m} \phi_{\text{eff}} \ln(\phi_{\text{eff}}) \right]^2}, \quad (27)$$

375 with $k_0 = 0.5$ being the geometrical parameter for spherical particles (Kozeny, 1927) and $\phi_c = 0.01$ as the critical porosity threshold. This threshold is lower than the published value of $\phi_c = 0.03$ (Van der Marck, 1996; Rintoul, 2000; Wadsworth et al., 2016). However, one of the subsamples do not feature continuous pathways, we compute the geometric mean of the permeability based on the results for all 8 subsamples (fig.5; inset). For this purpose we assume $k = 10^{-20} \text{ m}^2$ for subsamples without continuous pathways, referring to a nearly impermeable medium. The geometric mean shows that the computed permeabilities approach

380 ~~both the~~ used in this study had a porosity of 0.01 while still exhibiting a percolating cluster. For this reason, we here employed a critical porosity of $\phi_c = 0.01$.

With our parameterization for S , the permeability parameterization of Martys et al. (1994) reads as follows:

$$k = \frac{2[1 - \min(\phi_{\text{eff}}) - \phi_c]}{\left[-\frac{3}{3.8509 \times 10^{-4} m} \phi_{\text{eff}} \ln(\phi_{\text{eff}})\right]^2} [\min(\phi_{\text{eff}}) - \phi_c]^{4.2}, \quad (28)$$

385 From the grain size distribution of the glass beads used in this study (see Appendix D), we also determined the average grain diameter d and the harmonic mean diameter D , both within uncertainties equal to 1.20 mm. Inserting into the respective parameterizations of Revil and Cathles III (1999) and Garcia et al. (2009) (see (7) and eq.(8)) results in:

$$k = \frac{[1.20 \times 10^{-3} m]^2 \min(\phi_{\text{eff}})^{5.1}}{24}, \quad (29)$$

$$k = \min(\phi_{\text{eff}})^{0.11} [1.20 \times 10^{-3} m]^2 \quad (30)$$

390 The permeability parameterizations in general show similar trends but differ in the predicted permeability value. The Kozeny-Carman ~~curve and the measured permeabilities~~ relation shows good agreement with the experimentally measured samples, but also shows some offset towards the numerically computed values. A similarly good fit is obtained by the permeability parameterization of Martys et al. (1994). The parameterizations by Garcia et al. (2009) and Revil and Cathles III (1999) tend to underestimate permeability, which might be related to their assumptions on the samples heterogeneity.

395 ~~As discussed by previous studies the accuracy of permeability prediction improves with increasing numerical resolution (Gerke et al., 2018; Keehm, 2003; Eichheimer et al., 2019). To investigate this effect with respect to our samples, we computed the permeability of two subsamples (Ex35_04 & Ex36_02 see supplement material) using an increased resolution of 1024^3 grid points. The two samples with effective porosities at around 9 and 15% represent samples on both sides of the median of the present study's effective porosity range (1.5–22%). The permeability obtained using doubled grid resolution decreases only by around $\approx 2-4\%$ compared to the outcome of models with 512^3 grid resolution (see Appendix F). We are therefore confident that the calculations with 512^3 grid points provide sufficiently accurate results.~~

400

4 Discussion and conclusion

In this paper, we determine the permeability of nearly isotropic porous media ~~made out consisting~~ of sintered glass beads using a combined experimental-numerical approach. ~~By analyzing sample microstructures and the flow properties inside these samples, we are able to derive a modified Kozeny-Carman equation which improves theoretical permeability predictions~~ We analyzed sample microstructures using CT data and determined flow properties both experimentally and numerically. Using this data, we test different permeability parameterizations that have been proposed in the literature. The goal of this study was to particularly improve permeability parameterizations at low porosities ($<20\%$).

405

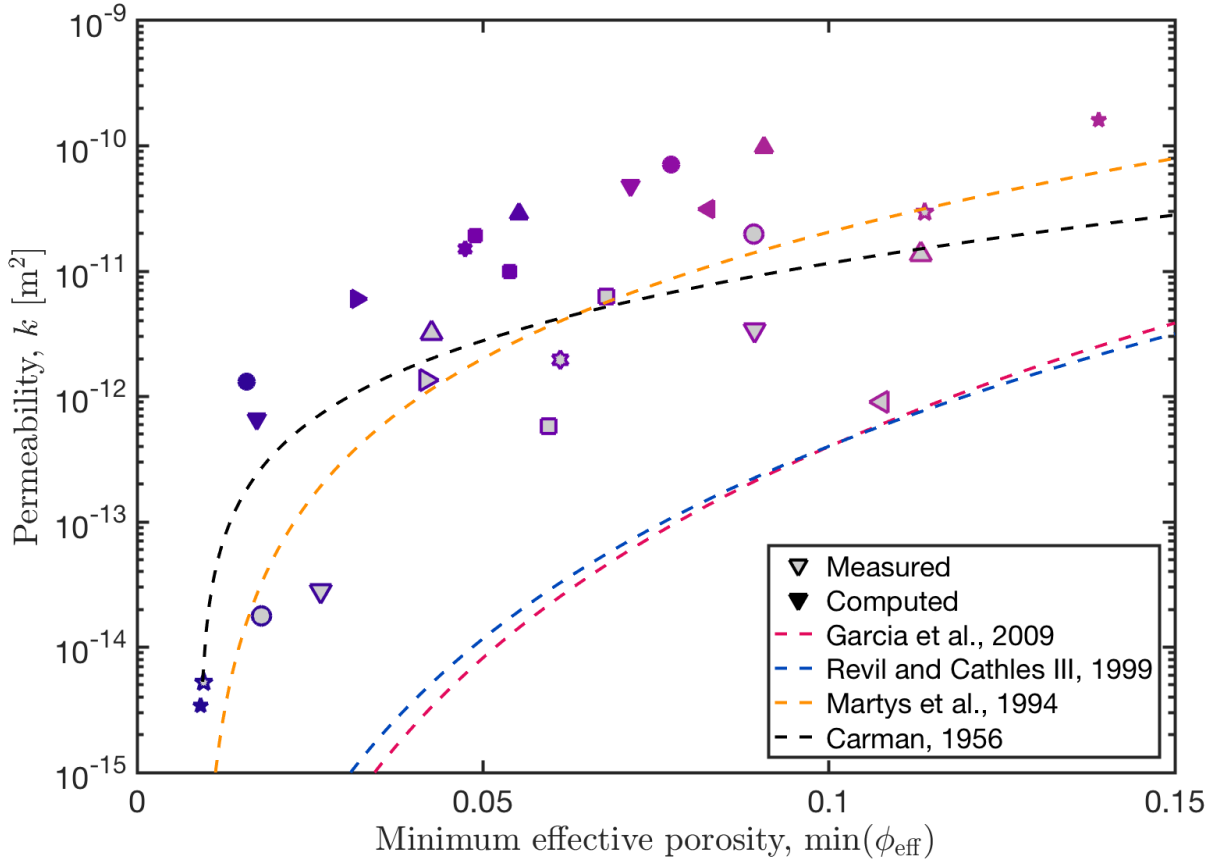


Figure 5. Computed and measured permeability against minimum effective porosity. Symbols of the same shape and color represent the same sample. Samples with grey face color represent measured values, whereas color only symbols stand for computed subsamples. The dotted black line (fit1) represents eq.(27) using computed permeabilities represent the arithmetic-geometric mean values of computed hydraulic tortuosities all subsamples. To verify existing permeability parameterizations, whereas we plotted the black dashed line (fit2) shows eq.(??) using relations of Revil and Cathles III (1999); Garcia et al. (2009); Carman (1956) and Martys et al. (1994) against the fitted linear curve for hydraulic tortuosity according to eq experimental and numerical permeabilities. Note that estimated errors for the experimental permeability measurements (??) tab. The inset displays 1a) are smaller than the geometric mean of the computed hydraulic tortuosities and measured values against effective porosity displayed symbols. Some subsamples with low effective porosity did not show a continuous pathway throughout the subsample, thus we assumed a very low permeability of 10^{-20} m^2 . Note that estimated errors for the experimental permeability measurements (tab.1) are smaller than the displayed symbols.

410 The computation of the Two particular microstructural parameters that we determined were the specific surface S and the hydraulic tortuosity τ_h . As these two parameters are frequently used in permeability parameterizations, we tested whether existing parameterizations are also valid in our case. We find that the effective specific surface shows a good fit using eq.(24)

from previous studies is well predicted by the parameterization eq.(24) proposed by Koponen et al. (1996), not only for the chosen subsamples but also for the full samples. The computed-fitted hydraulic radius of 0.385 mm is reasonable as the initial grain size of the glass beads is around 1 mm and the hydraulic pore radius of the glass beads is reduced during sample sintering.

415 Only few studies have investigated hydraulic tortuosity for three dimensional porous media (Du Plessis and Masliyah, 1991; Ahmadi et al., 2011; Backeberg et al., 2017). In previous studies As the hydraulic tortuosity was often assumed or used as fitting parameter as it is challenging to determine, in particular in experimental studies in experiments, experimental studies have often used this parameter as a fitting variable. Our data shows that contrary to suggestions by previous authors - contrary to previous suggestions - the hydraulic tortuosity does not change significantly with decreasing effective porosity (Matyka et al., 2008; Koponen et al., 1996; Mota et al., 2001), at least at the low porosities investigated in this study. We find an increasing scatter towards small effective porosities as the hydraulic tortuosity strongly depends on the sample microstructure. Using two dimensional squares Koponen et al. (1996) This observation agrees with the study by Koponen et al. (1996), but is at odds with the studies by Matyka et al. (2008) and Mota et al. (2001). The study by Koponen et al. (1996) was based on 2D numerical simulations and found hydraulic tortuosity values close to 2, whereas our data scatters lies around a value of 3. The difference between previous relations and our data is likely related to the different particle geometries used and that previous studies were done in 2D, while we employ 3D samples.

425

Using two dimensional squares the average hydraulic tortuosity of Koponen et al. (1996) is smaller than 2, but in general it displays a similar trend as our data. Our work shows that measured and computed permeability are Measured and computed permeabilities are generally in good agreement, but the computed permeability tends to yield with computed permeabilities consistently yielding towards higher values, whereas the measured permeability yields towards lower values in comparison to the permeability prediction using the than experimentally measured permeabilities. The experimental measured permeabilities show some scatter which might be related to heterogeneities within the sample. Interestingly, numerical permeability computations based on subsamples show much less scatter. Both the modified Kozeny-Carman equation. Differences between numerical and measured permeability might relation and the parameterization by Martys et al. (1994) predict numerically computed and experimentally measured permeability values well. In the modified Kozeny-Carman relation, hydraulic tortuosity seems to have a second order influence on the permeability of porous media. The permeability parameterizations by Revil and Cathles III (1999) and Garcia et al. (2009) underestimate permeabilities, which could be related to the fact that in order to be able to predict permeability numerically we employ subsamples as computational resources are limited. However, experimental measurements are carried out using the full sample. Thus in terms of permeability some of the subsamples seem not to be representative for the corresponding full sample. Furthermore increasing the numerical resolution affects the computed permeability only by assumptions used in these studies. It should be noted that Garcia et al. (2009) investigated heterogeneous sand packs and found that permeabilities for homogeneous packs are 1.6 – 1.8 times higher.

430

435

440

There are several reasons for the discrepancy between experimental and numerical values. First, numerical permeability predictions are based on simulations on subsamples, where free slip boundary conditions are employed. These boundary conditions do not accurately represent the flow field within the full sample and are therefore a possible source of error. This error can be estimated to about 20-50% of the computed value (Gerke et al., 2019). Second, the numerical computations compute

445

the flow field on a discretized grid with a given resolution. In particular at low porosities, pore structures may be too small to be well resolved by the grid. As discussed by previous studies the accuracy of permeability prediction improves with increasing numerical resolution (Gerke et al., 2018; Keehm, 2003; Eichheimer et al., 2019). To investigate this effect with respect to our samples, we computed the permeability of two subsamples (Ex35Sub04 and Ex36Sub02 see supplemental material) using an increased resolution of 1024^3 grid points. The two samples with effective porosities at around 9 and 15% represent samples on both sides of the median of the present study's effective porosity range (1.5 – 22%). The permeability obtained using doubled grid resolution decreases only by around $\approx 2 - 4\%$, demonstrating that subsamples compared to the outcome of models with 512^3 grid resolution (see Appendix F). We are therefore confident that the calculations with 512^3 pixels use a satisfactory numerical resolution. grid points provide sufficiently accurate results. To further increase the accuracy of the numerical computations, adaptive meshing methods could be useful.

~~Our study shows that by determining microstructural parameters the~~ Third and most important, it is not clear whether either the subsamples used in the numerical computations or the full samples used for experimental measurements can be considered representative volume elements at a certain porosity. The scatter that we observe in both numerical and experimental permeability measurements indicates that this may not be the case, in particular at porosities close to the critical porosity. A potential remedy for this issue would be the use of larger samples in both experiments and numerical simulations. However, using larger samples is not trivial. On the numerical side larger samples require significantly more computational resources. On the experimental side, larger samples reduce the resolution of the CT scans, which would in turn reduce the value of microstructural analysis. Additionally, a reduced CT resolution would also affect numerical permeability measurements.

We show that several permeability parameterizations (the modified Kozeny-Carman equation ~~can predict permeabilities for isotropic three-dimensional porous media (see eq. (??)). Using the fitted equations for effective specific surface and hydraulic tortuosity we provide a Kozeny-Carman equation for the estimation of permeability as input parameter in large-scale numerical models depending only on porosity . Furthermore predicting permeability for more complex porous media still remains challenging and needs to be investigated in future work~~ and the permeability parameterization by Martys et al. (1994)) are capable to predict the numerically and experimentally determined permeabilities obtained in our study. However, this could only be done by determining several microstructural parameters from CT scans and by modifying the respective equations to fit our data. In that respect, the parameterization by Martys et al. (1994) requires less fitting parameters, which makes it in our opinion preferable. However, our results also show a significant scatter in both numerical and experimental permeability measurements which are not predicted by either parameterization. This shows that further work is needed to obtain a more universal parameterization connecting microstructural parameters to permeability. To first order, the different permeability parameterizations can be used in numerical models to simulate fluid flow in isotropic low porosity media on the larger scale. However, it has to be kept in mind that rocks in nature are commonly more complex, as they (1) often consist of grains with different shapes and sizes, (2) contain fractures which serve as preferred pathways for fluid flow and (3) often also contain anisotropic structures.

~~This~~ Nevertheless, our study demonstrates that numerical permeability computations can complement laboratory measurements, in particular in cases of small sample sizes or effective porosities $< 5\%$. ~~Furthermore we~~ We provide segmented input

files of several samples with different porosities ~~-. This should allow other workers to use these input in the supplementary. We hope that this will allow other researchers to use this~~ data and our results to benchmark other numerical methods in the future.

Code availability. <https://bitbucket.org/bkaus/lamem/src/master/>; commit: 9c06e4077439b5492d49d03c27d3a1a5f9b65d32 (Popov and Kaus, 485 2016).

Data availability. Detailed data tables for each sample can be found in the supplementary material. The segmented CT images of three samples with different porosities are provided using the figshare repository (doi:10.6084/m9.figshare.11378517).

Appendix A: Minimum effective porosity

This figure shows the comparison between the effective porosity and the minimum effective porosity, which may control the fluid flow within the sample. The minimum effective porosity is used in fig.5.

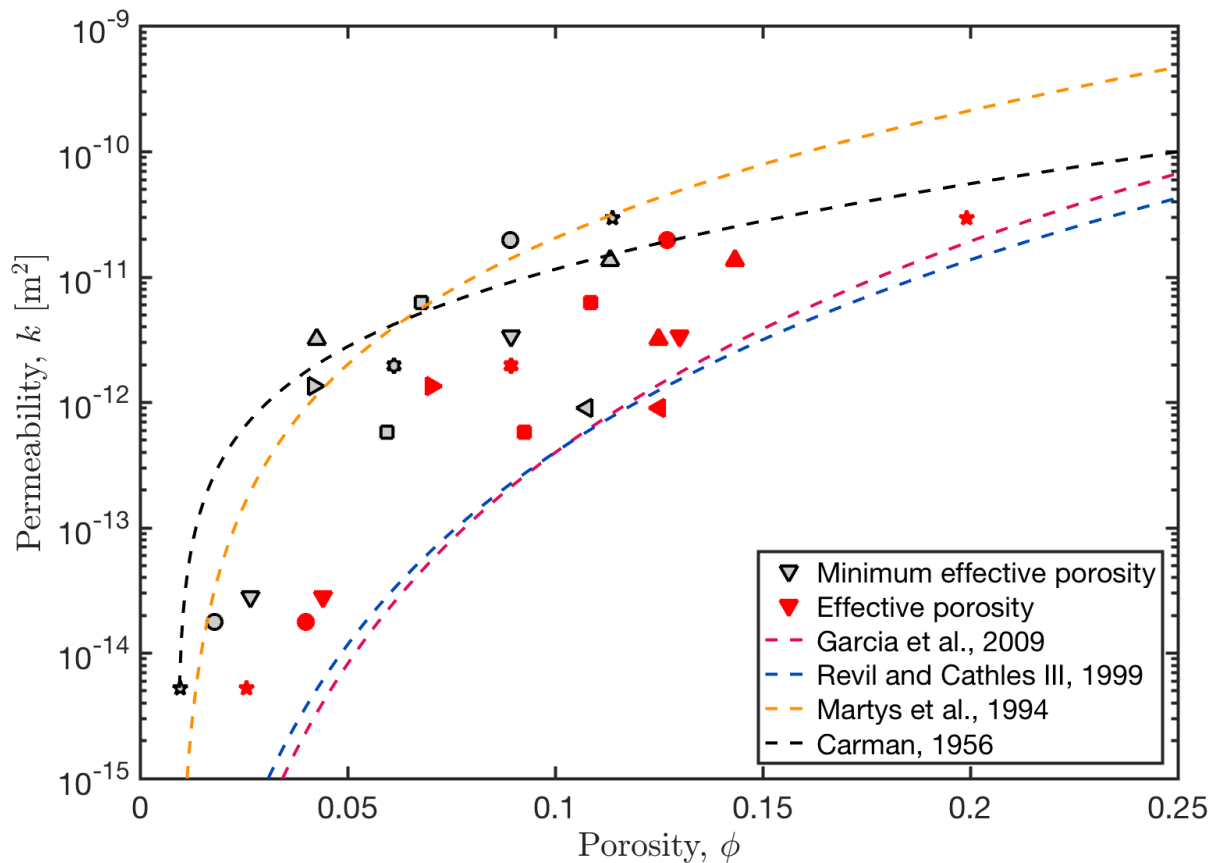


Figure A1. Measured permeability against porosity. Symbols with grey face color represent sample using the minimum effective porosity per sample, while red symbols display measured sample using the effective porosity. Dashed lines show several permeability parameterizations.

Appendix B: Permeability of each subsample

This figure shows the computed permeability of each subsample together with the measured permeability values and the permeability parameterizations.

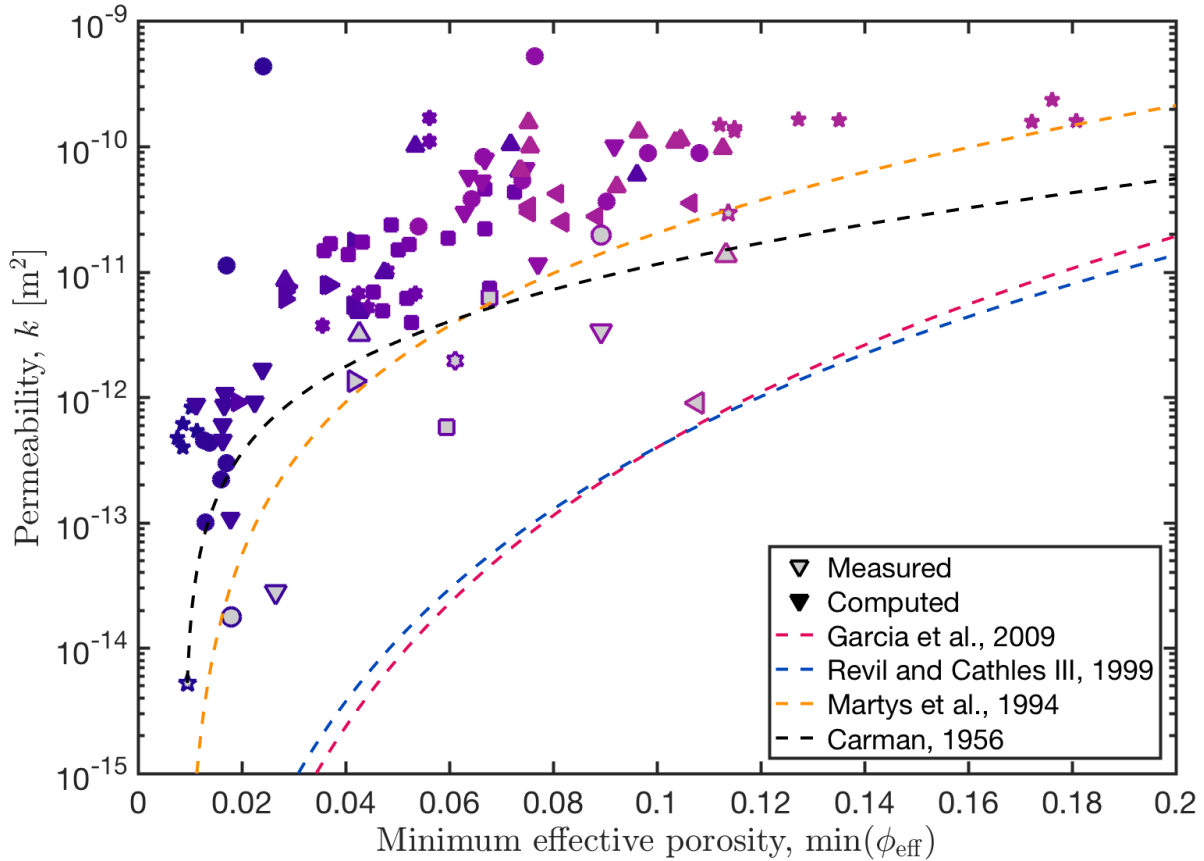


Figure B1. Computed and measured permeability against minimum effective porosity. Symbols of the same shape and color represent the same sample. Samples with grey face color represent measured values, whereas color only symbols stand for computed subsamples. To verify existing permeability parameterizations, we plotted the relations of Revil and Cathles III (1999); Garcia et al. (2009); Carman (1956) and Martys et al. (1994) against the experimental and numerical permeabilities. Note that estimated errors for the experimental permeability measurements (tab.1a) are smaller than the displayed symbols.

Appendix C: Applicability of Darcy's Law

495 For the numerical permeability computation using the Stokes equations we assume laminar flow conditions and incompressibility. Laminar flow conditions are represented by a linear relationship between applied pressure gradient and flow rate (fig.C1). Regarding the incompressibility of the working gas during the measurements we computed permeabilities using both Darcy's law (eq.(1)) and Darcy's law for compressible gas as follows (Takeuchi et al., 2008):

$$\frac{P_2^2 - P_1^2}{2P_2L} = \frac{\eta\nu_0}{k}, \quad (C1)$$

500 with P_2 and P_1 being the pressures at the inlet and outlet side of the sample respectively, and ν_0 being the volume flux, which is calculated from the flow rate divided by cross-sectional area of the sample. The left-hand side of Eq.(C1) represents the modified pressure gradient that includes the compressibility of working gas. The difference between both computed permeabilities is less than 10%, we therefore assume the effect of compressibility to be minor.

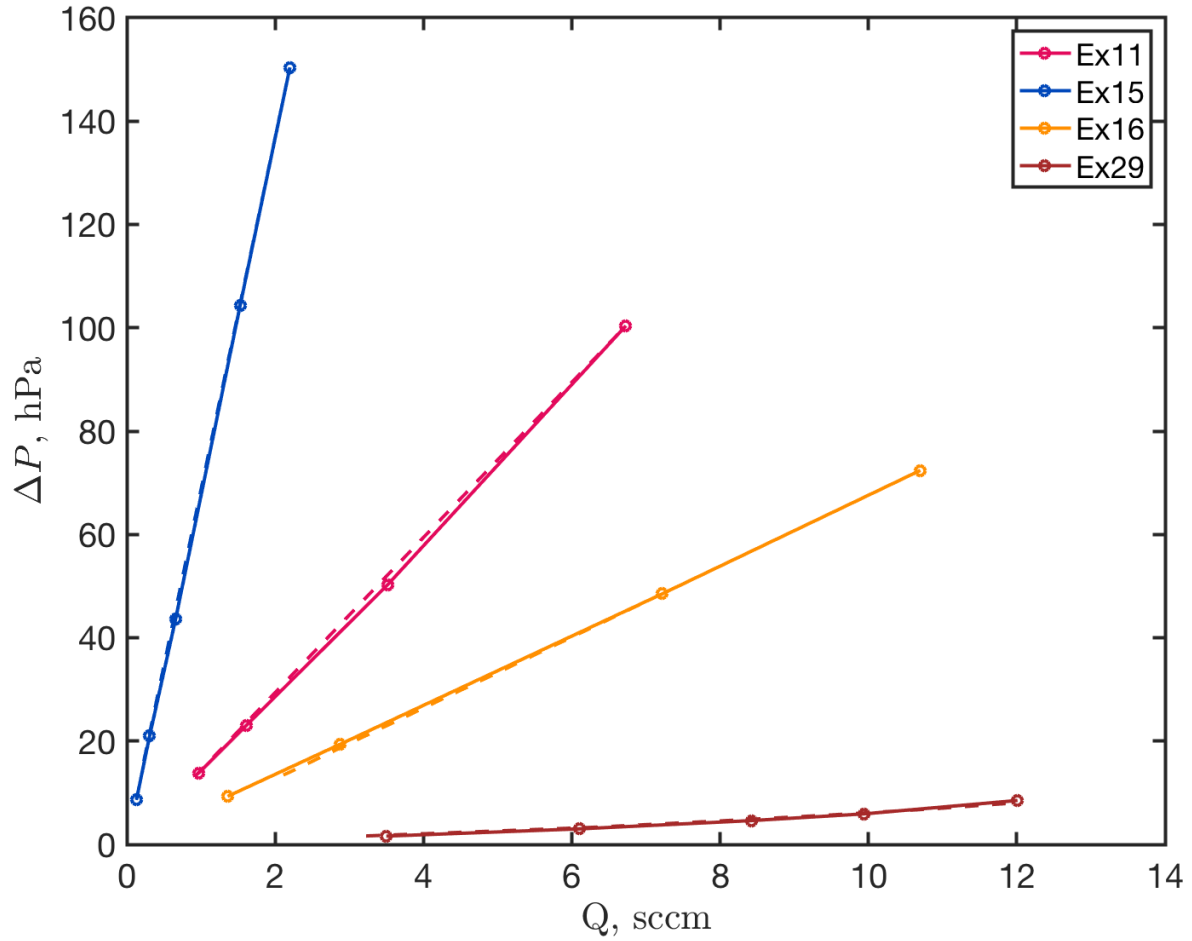


Figure C1. The linear relations between applied pressure difference and flow rate show that Darcy's law is valid and no turbulent flow occurs. Solid lines represent measurements while increasing the pressure gradient-difference and dashed lines while decreasing the pressure gradient-difference. The unit of *sccm* refers to a standard cubic centimeter per minute.

Appendix D: Grain size distribution of used glass beads

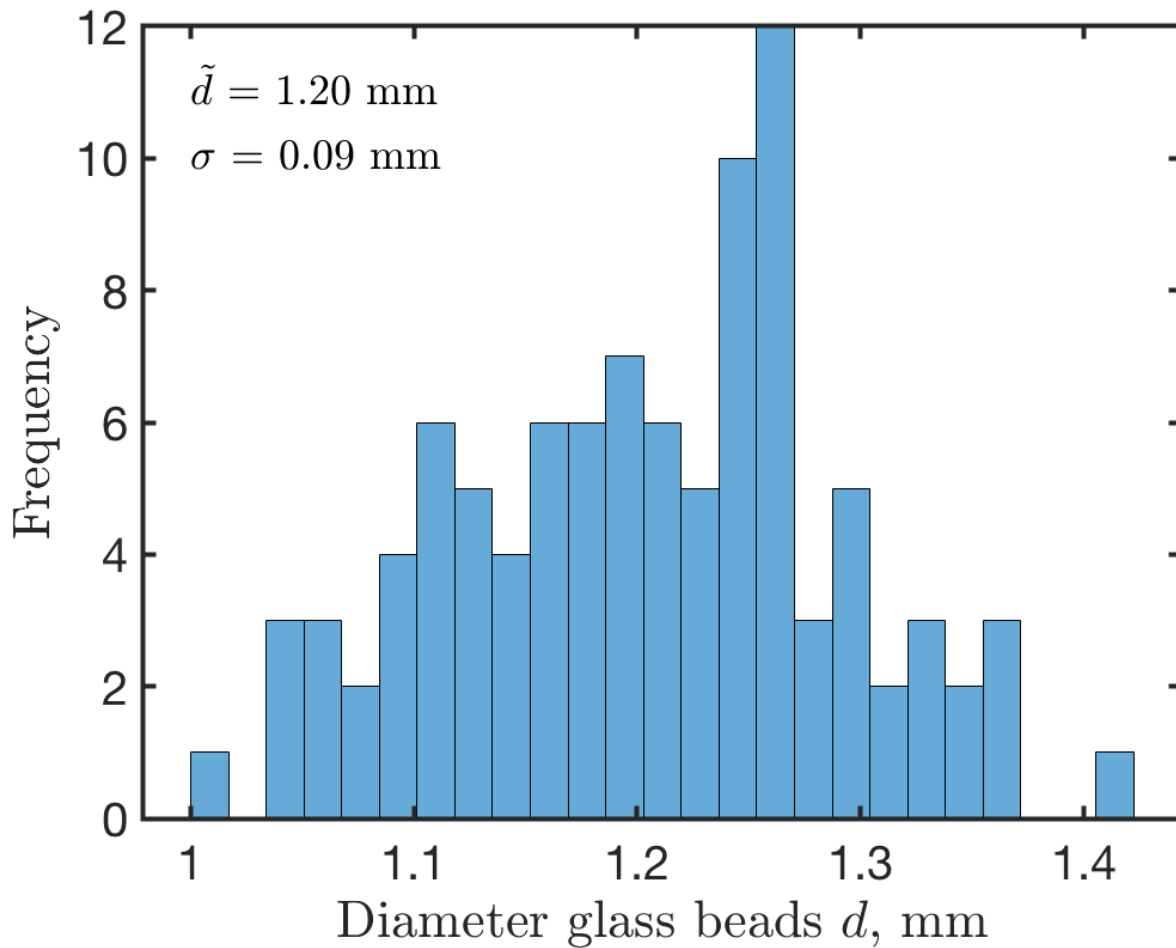


Figure D1. Size frequency distribution of the glass beads diameter. Beside the distribution, both the arithmetic mean \tilde{d} and standard deviation σ are given.

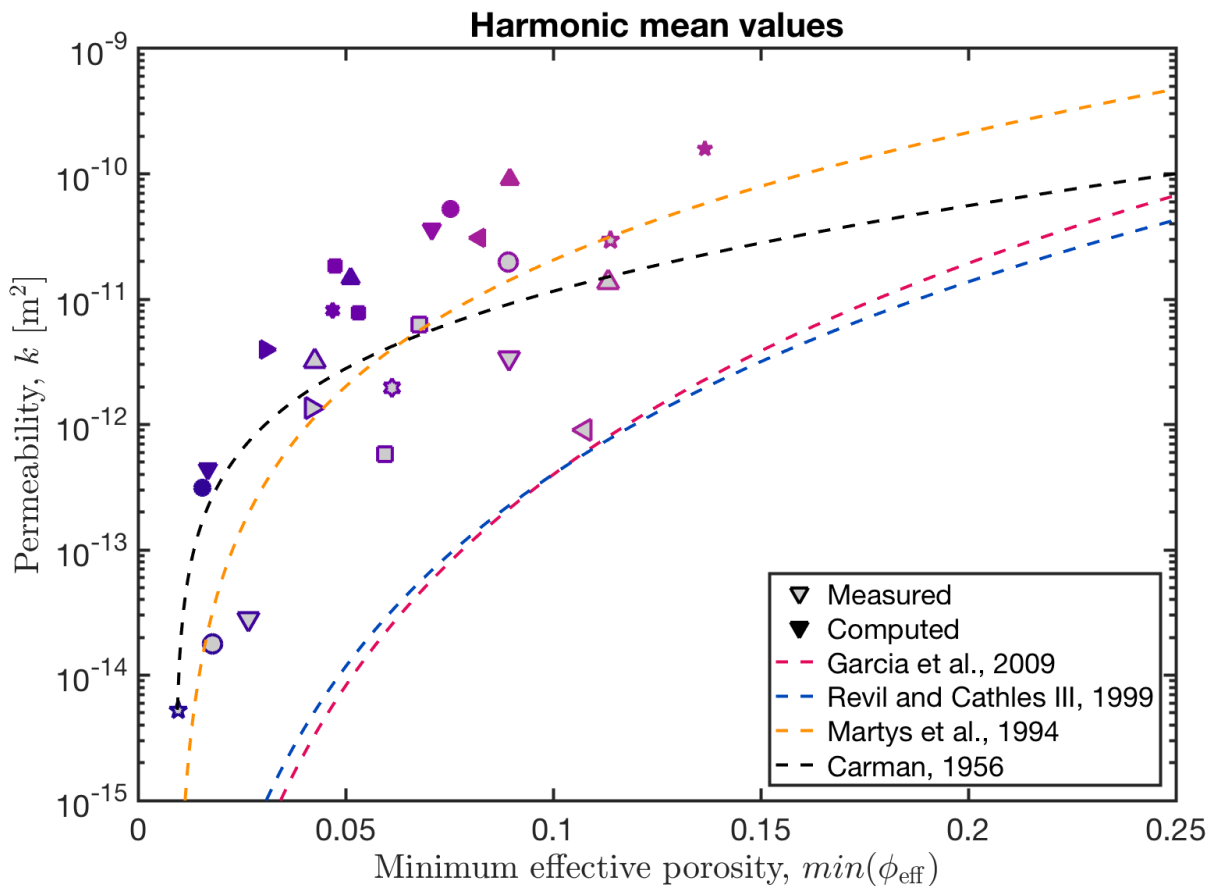


Figure E1. [Computed and measured permeability against minimum effective porosity.](#) [Symbols of the same shape and color represent the same sample.](#) [Samples with grey face color represent measured values, whereas color only symbols stand for computed subsamples.](#) [The computed permeabilities represent the harmonic mean values of all subsamples.](#) [To verify existing permeability parameterizations, we plotted the relations of Revil and Cathles III \(1999\); Garcia et al. \(2009\); Carman \(1956\) and Martys et al. \(1994\) against the experimental and numerical permeabilities.](#) [Note that estimated errors for the experimental permeability measurements \(tab.1a\) are smaller than the displayed symbols.](#)

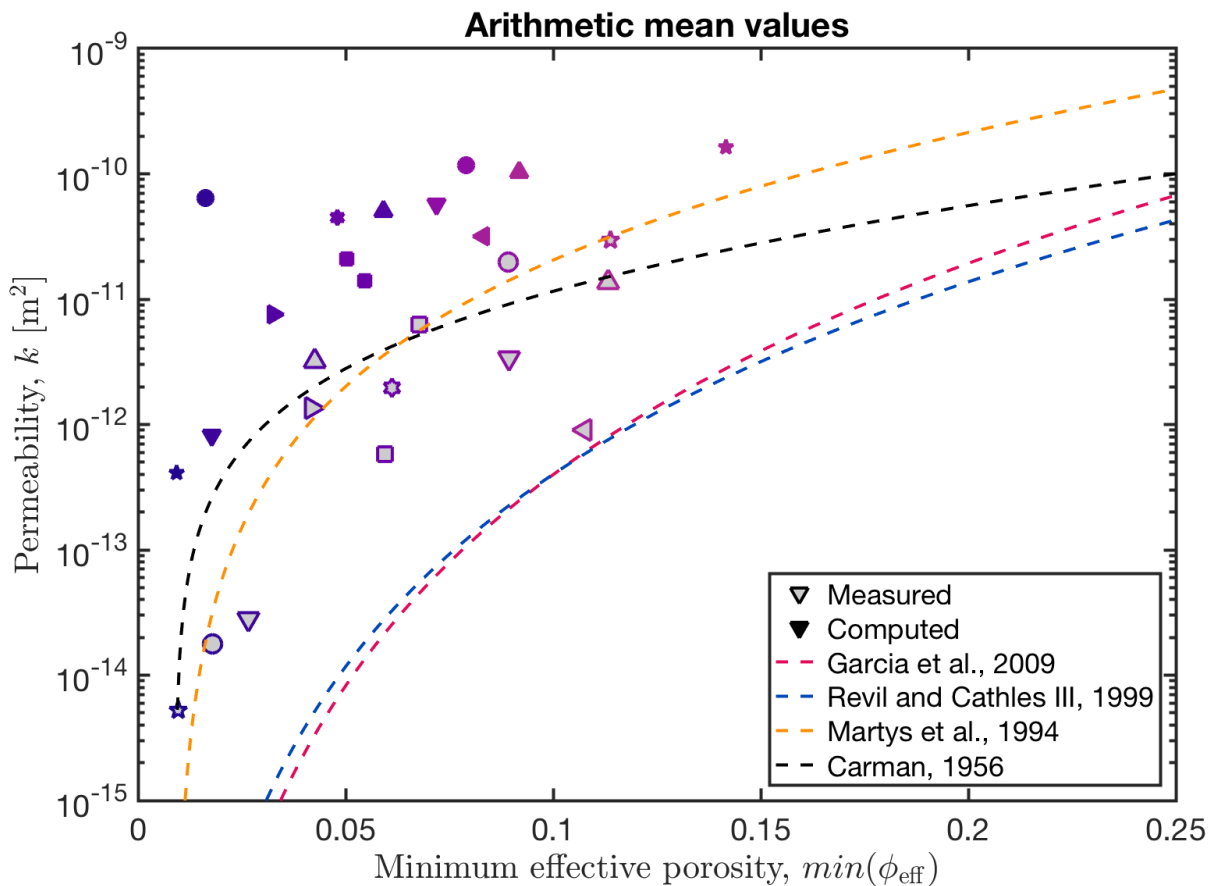


Figure E2. Computed and measured permeability against minimum effective porosity. Symbols of the same shape and color represent the same sample. Samples with grey face color represent measured values, whereas color only symbols stand for computed subsamples. The computed permeabilities represent the arithmetic mean values of all subsamples. To verify existing permeability parameterizations, we plotted the relations of Revil and Cathles III (1999); Garcia et al. (2009); Carman (1956) and Martys et al. (1994) against the experimental and numerical permeabilities. Note that estimated errors for the experimental permeability measurements (tab.1a) are smaller than the displayed symbols.

Appendix F: Resolution test

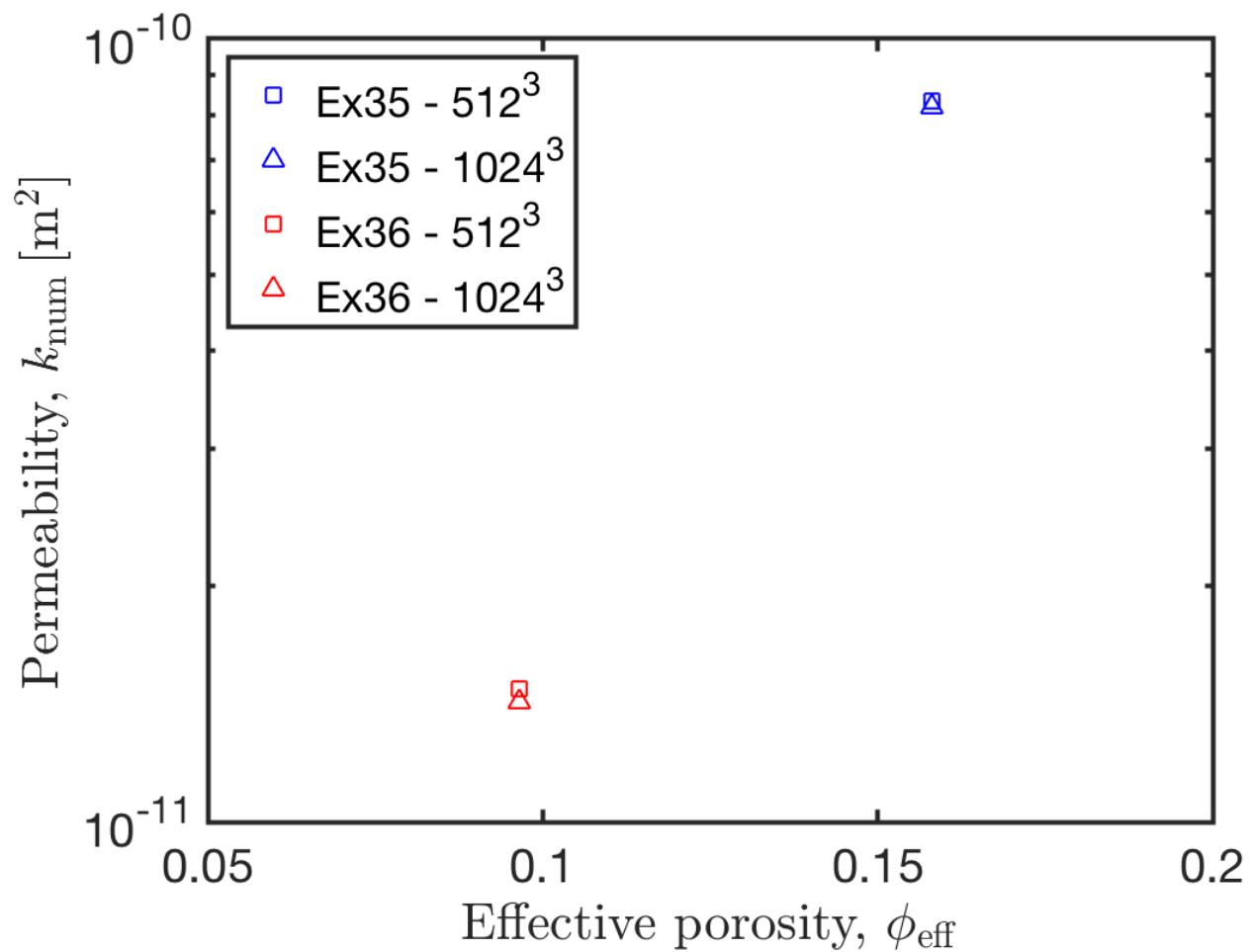


Figure F1. Resolution test using samples [Ex35sub04](#) [Ex35Sub04](#) and [Ex36sub02](#) [Ex36Sub02](#) (for details see also tables in the supplement). Colored squares denote standard resolution of 512³, whereas colored triangles are simulations with resolution of 1024³ voxels.

Appendix G: Critical porosity threshold

510 The samples employed in the present study display a critical porosity threshold of 0.015. In case the spheres are all similarly packed and there should be no critical porosity threshold as the geometrical dihedral angle between the spherical grains and air should be much smaller than 60° . In the actual experimental products, however, the boundary between the softened soda-lime glass beads started to heal by (i) expelling the air and (ii) element diffusion between the glass beads, resulting in the decrease of the interfacial tension force and increase of the dihedral angle as observed in the crack healing in supercooled melts (Yoshimura and Nakamura, 2010). This way some pathways are expected to pinch-off and thus form both rugby ball-shaped isolated pockets and cigar-shaped dead-ends (see fig.??). While the isolated pores were excluded in our calculations, the
515 dead-ends are expected to cause the critical porosity threshold. The CT slice highlights several structural features forming the critical porosity threshold.

Author contributions. PE contributed in designing the study, sample preparation and permeability measurements. Furthermore PE did visualization, writing, methodology and running simulations. MT contributed in data interpretation, methodology, designing the study and manuscript writing. WF performed sample preparation and permeability measurements. GJG contributed in designing the study, data
520 interpretation and manuscript writing. MN designed the study and contributed in data interpretation. SO contributed in sample preparation and measurements. TK sintered the glass bead porous media. MOK performed the resolution test. All authors contributed in writing and improving the manuscript.

Competing interests. The authors declare that they have no conflict of interest.

Acknowledgements. This work has been supported by DFG (grant no. GRK 2156/1), the JSPS Japanese-German graduate externship and
525 BMBF (grant no. 03G0865A). M.T. was supported by the Bayerisches Geoinstitut Visitors Program. Calculations were performed on clusters btrzx2, University of Bayreuth and Mogon II, Johannes Gutenberg University Mainz. [We thank Kirill Gerke and an anonymous reviewer for their constructive comments that helped to improve the manuscript considerably.](#)

References

- Ahmadi, M. M., Mohammadi, S., and Hayati, A. N.: Analytical derivation of tortuosity and permeability of monosized spheres: A volume averaging approach, *Phys. Rev. E*, 83, 026312, <https://doi.org/10.1103/PhysRevE.83.026312>, 2011.
- 530 Andrä, H., Combaret, N., Dvorkin, J., Glatt, E., Han, J., Kabel, M., Keehm, Y., Krzikalla, F., Lee, M., Madonna, C., Marsh, M., Mukerji, T., Saenger, E. H., Sain, R., Saxena, N., Ricker, S., Wiegmann, A., and Zhan, X.: Digital rock physics benchmarks—Part I: Imaging and segmentation, *Computers & Geosciences*, 50, 25 – 32, <https://doi.org/doi.org/10.1016/j.cageo.2012.09.005>, 2013b.
- Andrä, H., Combaret, N., Dvorkin, J., Glatt, E., Han, J., Kabel, M., Keehm, Y., Krzikalla, F., Lee, M., Madonna, C., Marsh, M., Mukerji, T., Saenger, E. H., Sain, R., Saxena, N., Ricker, S., Wiegmann, A., and Zhan, X.: Digital rock physics benchmarks—Part II: Computing effective properties, *Computers & Geosciences*, 50, 33 – 43, <https://doi.org/https://doi.org/10.1016/j.cageo.2012.09.008>, 2013a.
- 535 Arns, C. H.: A comparison of pore size distributions derived by NMR and X-ray-CT techniques, *Physica A: Statistical Mechanics and its Applications*, 339, 159–165, <https://doi.org/10.1016/j.physa.2004.03.033>, 2004.
- Arns, C. H., Knackstedt, M. A., Pinczewski, M. V., and Lindquist, W.: Accurate estimation of transport properties from microtomographic images, *Geophysical Research Letters*, 28, 3361–3364, <https://doi.org/10.1029/2001GL012987>, 2001.
- 540 Azar, J. H., Javaherian, A., Pishvaie, M. R., and Nabi-Bidhendi, M.: An approach to defining tortuosity and cementation factor in carbonate reservoir rocks, *Journal of Petroleum Science and Engineering*, 60, 125 – 131, <https://doi.org/10.1016/j.petrol.2007.05.010>, 2008.
- Backeberg, N. R., Lacoviello, F., Rittner, M., Mitchell, T. M., Jones, A. P., Day, R., Wheeler, J., Shearing, P. R., Vermeesch, P., and Striolo, A.: Quantifying the anisotropy and tortuosity of permeable pathways in clay-rich mudstones using models based on X-ray tomography, *Scientific Reports*, 7, 14838, <https://doi.org/10.1038/s41598-017-14810-1>, 2017.
- 545 Balay, S., Abhyankar, S., Adams, M. F., Brown, J., Brune, P., Buschelman, K., Dalcin, L., Dener, A., Eijkhout, V., Gropp, W. D., Karpeyev, D., Kaushik, D., Knepley, M. G., May, D. A., McInnes, L. C., Mills, R. T., Munson, T., Rupp, K., Sanan, P., Smith, B. F., Zampini, S., Zhang, H., and Zhang, H.: PETSc Users Manual, Tech. Rep. ANL-95/11 - Revision 3.12, Argonne National Laboratory, <https://www.mcs.anl.gov/petsc>, 2019.
- 550 Bear, J.: *Dynamics of Fluids in Porous Media*, Dover Publications Inc., New York, 1988.
- Bekins, B. A. and Dreiss, S. J.: A simplified analysis of parameters controlling dewatering in accretionary prisms, *Earth and Planetary Science Letters*, 109, 275 – 287, [https://doi.org/https://doi.org/10.1016/0012-821X\(92\)90092-A](https://doi.org/https://doi.org/10.1016/0012-821X(92)90092-A), 1992.
- Berg, R. R.: Capillary Pressures in Stratigraphic Traps, *AAPG Bulletin*, 59, 939–956, <https://doi.org/10.1306/83D91EF7-16C7-11D7-8645000102C1865D>, 1975.
- 555 Bernabe, Y., Brace, W., and Evans, B.: Permeability, porosity and pore geometry of hot-pressed calcite, *Mechanics of Materials*, 1, 173 – 183, [https://doi.org/https://doi.org/10.1016/0167-6636\(82\)90010-2](https://doi.org/https://doi.org/10.1016/0167-6636(82)90010-2), 1982.
- Bernabé, Y., Li, M., and Maineult, A.: Permeability and pore connectivity: A new model based on network simulations, *Journal of Geophysical Research: Solid Earth*, 115, <https://doi.org/10.1029/2010JB007444>, 2010.
- Bird, M., Butler, S. L., Hawkes, C., and Kotzer, T.: Numerical modeling of fluid and electrical currents through geometries based on synchrotron X-ray tomographic images of reservoir rocks using Avizo and COMSOL, *Computers & Geosciences*, 73, 6–16, <https://doi.org/10.1016/j.cageo.2014.08.009>, 2014.
- 560 Bird, R., Stewart, W., and Lightfoot, E.: *Transport Phenomena*, New York, London: Wiley, revised second Edition, 2006.
- Bosl, W. J., Dvorkin, J., and Nur, A.: A study of porosity and permeability using a lattice Boltzmann simulation, *Geophysical Research Letters*, 25, 1475–1478, <https://doi.org/10.1029/98GL00859>, 1998.

- 565 Bourbie, T., Coussy, O., Zinszner, B., and Junger, M. C.: Acoustics of Porous Media, *The Journal of the Acoustical Society of America*, 91, 3080–3080, 1992.
- Brace, W. F.: Permeability of crystalline and argillaceous rocks, *International Journal of Rock Mechanics and Mining Sciences & Geomechanics Abstracts*, 17, 241–251, [https://doi.org/10.1016/0148-9062\(80\)90807-4](https://doi.org/10.1016/0148-9062(80)90807-4), 1980.
- Carman, P. C.: Fluid flow through granular beds, *Trans. Inst. Chem. Eng.*, 15, 150–166, 1937.
- 570 Carman, P. C.: Flow of gases through porous media, New York, Academic Press, 1956.
- Chapuis, R. P. and Aubertin, M.: On the use of the Kozeny–Carman equation to predict the hydraulic conductivity of soils, *Canadian Geotechnical Journal*, 40, 616–628, <https://doi.org/10.1139/t03-013>, 2003.
- Clennell, M. B.: Tortuosity: A guide through the maze, Geological Society, London, Special Publications, 122, 299–344, 1997.
- Collinson, A. and Neuberg, J.: Gas storage, transport and pressure changes in an evolving permeable volcanic edifice, *Journal of Volcanology and Geothermal Research*, 243–244, 1 – 13, <https://doi.org/https://doi.org/10.1016/j.jvolgeores.2012.06.027>, 2012.
- 575 Comiti, J. and Renaud, M.: A new model for determining mean structure parameters of fixed beds from pressure drop measurements: application to beds packed with parallelepipedal particles, *Chemical Engineering Science*, 44, 1539 – 1545, [https://doi.org/https://doi.org/10.1016/0009-2509\(89\)80031-4](https://doi.org/https://doi.org/10.1016/0009-2509(89)80031-4), 1989.
- Darcy, H. P. G.: Les Fontaines publiques de la ville de Dijon: exposition et application des principes à suivre et des formules à employer dans les questions de distribution d’eau., Paris: V. Dalmont, 1856.
- 580 Domenico, P. A. and Schwartz, F. W.: Physical and chemical hydrogeology, Wiley, New York, 1998.
- Du Plessis, J. P. and Masliyah, J. H.: Flow through isotropic granular porous media, *Transport in Porous Media*, 6, 207–221, <https://doi.org/10.1007/BF00208950>, 1991.
- Dvorkin, J., Derzhi, N., Diaz, E., and Fang, Q.: Relevance of computational rock physics, *Geophysics*, 76, E141–E153, <https://doi.org/10.1190/geo2010-0352.1>, 2011.
- 585 Eichheimer, P., Thielmann, M., Popov, A., Golabek, G. J., Fujita, W., Kottwitz, M. O., and Kaus, B. J. P.: Pore-scale permeability prediction for Newtonian and non-Newtonian fluids, *Solid Earth*, 10, 1717–1731, <https://doi.org/10.5194/se-10-1717-2019>, 2019.
- Fehn, U. and Cathles, L. M.: Hydrothermal convection at slow-spreading mid-ocean ridges, *Tectonophysics*, 55, 239–260, [https://doi.org/10.1016/0040-1951\(79\)90343-3](https://doi.org/10.1016/0040-1951(79)90343-3), 1979.
- 590 Garcia, X., Akanji, L. T., Blunt, M. J., Matthai, S. K., and Latham, J. P.: Numerical study of the effects of particle shape and polydispersity on permeability, *Phys. Rev. E*, 80, 021 304, <https://doi.org/10.1103/PhysRevE.80.021304>, 2009.
- Gerke, K. M., Vasilyev, R. V., Khirevich, S., Collins, D., Karsanina, M. V., Sizonenko, T. O., Korost, D. V., Lamontagne, S., and Mallants, D.: Finite-difference method Stokes solver (FDMSS) for 3D pore geometries: Software development, validation and case studies, *Computers & Geosciences*, 114, 41–58, <https://doi.org/10.1016/j.cageo.2018.01.005>, 2018.
- 595 Gerke, K. M., Karsanina, M. V., and Katsman, R.: Calculation of tensorial flow properties on pore level: Exploring the influence of boundary conditions on the permeability of three-dimensional stochastic reconstructions, *Phys. Rev. E*, 100, 053 312, <https://doi.org/10.1103/PhysRevE.100.053312>, 2019.
- Ghanbarian, B., Hunt, A. G., Ewing, R. P., and Sahimi, M.: Tortuosity in porous media: A critical review, *Soil science society of America journal*, 77, 1461–1477, 2013.
- 600 Gleeson, T. and Ingebritsen, S. E.: Crustal Permeability, John Wiley & Sons, Ltd, <https://doi.org/10.1002/9781119166573>, 2016.
- Harlow, F. H. and Welch, J. E.: Numerical Calculation of Time-Dependent Viscous Incompressible Flow of Fluid with Free Surface, *The Physics of Fluids*, 8, 2182–2189, <https://doi.org/10.1063/1.1761178>, 1965.

- Hendraningrat, L., Li, S., and Torsæter, O.: A coreflood investigation of nanofluid enhanced oil recovery, *Journal of Petroleum Science and Engineering*, 111, 128 – 138, <https://doi.org/10.1016/j.petrol.2013.07.003>, 2013.
- 605 Hernández-López, M. F., Gironás, J., Braud, I., Suárez, F., and Muñoz, J. F.: Assessment of evaporation and water fluxes in a column of dry saline soil subject to different water table levels, *Hydrological Processes*, 28, 3655–3669, <https://doi.org/10.1002/hyp.9912>, 2014.
- Hölting, B. and Coldewey, W. G.: *Hydrogeology*, Springer-Verlag GmbH, Berlin, <https://doi.org/10.1007/978-3-662-56375-5>, 2019.
- Honarpour, M. M.: *Relative Permeability Of Petroleum Reservoirs*: Boca Raton, Florida, CRC press, 2018.
- Jang, J., Narsilio, G. A., and Santamarina, J. C.: Hydraulic conductivity in spatially varying media—a pore-scale investigation, *Geophysical Journal International*, 184, 1167–1179, <https://doi.org/10.1111/j.1365-246X.2010.04893.x>, 2011.
- 610 Kaus, B. J. P., Popov, A. A., Baumann, T. S., Püsök, A. E., Bauville, A., Fernandez, N., and Collignon, M.: Forward and Inverse Modelling of Lithospheric Deformation on Geological Timescales, *NIC Series*, 48, 299–307, 2016.
- Keehm, Y.: *Computational rock physics: Transport properties in porous media and applications*, Ph.D. thesis, Stanford University, 2003.
- Keller, T. and Katz, R. F.: The Role of Volatiles in Reactive Melt Transport in the Asthenosphere, *Journal of Petrology*, 57, 1073–1108, 615 <https://doi.org/10.1093/petrology/egw030>, 2016.
- Keller, T. and Suckale, J.: A continuum model of multi-phase reactive transport in igneous systems, *Geophysical Journal International*, 219, 185–222, <https://doi.org/10.1093/gji/ggz287>, 2019.
- Klug, C. and Cashman, K. V.: Permeability development in vesiculating magmas: implications for fragmentation, *Bulletin of Volcanology*, 58, 87–100, <https://doi.org/10.1007/s004450050128>, 1996.
- 620 Koponen, A., Kataja, M., and Timonen, J. v.: Tortuous flow in porous media, *Physical Review E*, 54, 406–410, <https://doi.org/10.1103/PhysRevE.54.406>, 1996.
- Koponen, A., Kataja, M., and Timonen, J.: Permeability and effective porosity of porous media, *Phys. Rev. E*, 56, 3319–3325, <https://doi.org/10.1103/PhysRevE.56.3319>, 1997.
- Kozeny, J.: Über kapillare Leitung des Wassers im Boden, *Royal Academy of Science, Vienna, Proc. Class I*, 136, 271–306, 1927.
- 625 Kuczynski, G. C.: Study of the Sintering of Glass, *Journal of Applied Physics*, 20, 1160–1163, 1949.
- Lamur, A., Kendrick, J. E., Eggertsson, G. H., Wall, R. J., Ashworth, J. D., and Lavallée, Y.: The permeability of fractured rocks in pressurised volcanic and geothermal systems, *Scientific Reports*, 7, 6173, <https://doi.org/10.1038/s41598-017-05460-4>, 2017.
- Manickam, S. S., Gelb, J., and McCutcheon, J. R.: Pore structure characterization of asymmetric membranes: Non-destructive characterization of porosity and tortuosity, *Journal of Membrane Science*, 454, 549 – 554, <https://doi.org/10.1016/j.memsci.2013.11.044>, 2014.
- 630 Manwart, C., Aaltosalmi, U., Koponen, A., Hilfer, R., and Timonen, J.: Lattice-Boltzmann and finite-difference simulations for the permeability for three-dimensional porous media, *Physical Review E*, 66, 016 702, <https://doi.org/10.1103/PhysRevE.66.016702>, 2002.
- Martys, N. S., Torquato, S., and Bentz, D. P.: Universal scaling of fluid permeability for sphere packings, *Phys. Rev. E*, 50, 403–408, <https://doi.org/10.1103/PhysRevE.50.403>, 1994.
- Matyka, M., Khalili, A., and Koza, Z.: Tortuosity-porosity relation in porous media flow, *Physical Review E*, 78, 026 306, 635 <https://doi.org/10.1103/PhysRevE.78.026306>, 2008.
- Mavko, G. and Nur, A.: The effect of a percolation threshold in the Kozeny-Carman relation, *Geophysics*, 62, 1480–1482, <https://doi.org/10.1190/1.1444251>, 1997.
- Miller, K. J., lu Zhu, W., Montési, L. G., and Gaetani, G. A.: Experimental quantification of permeability of partially molten mantle rock, *Earth and Planetary Science Letters*, 388, 273 – 282, <https://doi.org/https://doi.org/10.1016/j.epsl.2013.12.003>, 2014.

- 640 Morais, A. F., Seybold, H., Herrmann, H. J., and Andrade, J. S.: Non-Newtonian Fluid Flow through Three-Dimensional Disordered Porous Media, *Phys. Rev. Lett.*, 103, 194 502, <https://doi.org/10.1103/PhysRevLett.103.194502>, 2009.
- Mostaghimi, P., Blunt, M. J., and Bijeljic, B.: Computations of Absolute Permeability on Micro-CT Images, *Mathematical Geosciences*, 45, 103–125, <https://doi.org/10.1007/s11004-012-9431-4>, 2013.
- Mota, M., Teixeira, J. A., Bowen, W. R., and Yelshin, A.: Binary spherical particle mixed beds: porosity and permeability relationship
645 measurement, 17, 101–106, 2001.
- Mueller, S., Melnik, O., Spieler, O., Scheu, B., and Dingwell, D. B.: Permeability and degassing of dome lavas undergoing rapid decompression: An experimental determination, *Bulletin of Volcanology*, 67, 526–538, <https://doi.org/10.1007/s00445-004-0392-4>, 2005.
- Napolitano, A. and Hawkins, E. G.: Viscosity of a standard soda-lime-silica glass, *J. Res. Nat. Bur. Stand. A*, 68, 439–448, 1964.
- Nemati, R., Shahrouzi, J. R., and Alizadeh, R.: A stochastic approach for predicting tortuosity in porous media via pore network modeling,
650 *Computers and Geotechnics*, 120, 103 406, <https://doi.org/10.1016/j.compgeo.2019.103406>, 2020.
- Norton, D. and Taylor Jr, H. P.: Quantitative Simulation of the Hydrothermal Systems of Crystallizing Magmas on the Basis of Transport Theory and Oxygen Isotope Data: An analysis of the Skaergaard intrusion, *Journal of Petrology*, 20, 421–486, <https://doi.org/10.1093/petrology/20.3.421>, 1979.
- Okumura, S. and Sasaki, O.: Permeability reduction of fractured rhyolite in volcanic conduits and its control on eruption cyclicality, *Geology*,
655 42, 843–846, <https://doi.org/10.1130/G35855.1>, 2014.
- Okumura, S., Nakamura, M., Takeuchi, S., Tsuchiyama, A., Nakano, T., and Uesugi, K.: Magma deformation may induce non-explosive volcanism via degassing through bubble networks, *Earth and Planetary Science Letters*, 281, 267 – 274, <https://doi.org/https://doi.org/10.1016/j.epsl.2009.02.036>, 2009.
- Osorno, M., Uribe, D., Ruiz, O. E., and Steeb, H.: Finite difference calculations of permeability in large domains in a wide porosity range,
660 *Archive of Applied Mechanics*, 85, 1043–1054, <https://doi.org/10.1007/s00419-015-1025-4>, 2015.
- Otsu, N.: A threshold selection method from gray-level histograms, *IEEE transactions on systems, man, and cybernetics*, 9, 62–66, 1979.
- Pape, H., Clauser, C., and Iffland, J.: Permeability prediction for reservoir sandstones and basement rocks based on fractal pore space geometry, pp. 1032–1035, *Society of Exploration Geophysicists*, <https://doi.org/10.1190/1.1820060>, 2005.
- Pech, D.: Etude de la perméabilité de lits compressibles constitués de copeaux de bois partiellement déstructurés, Ph.D. thesis, INP Grenoble,
665 1984.
- Popov, A. and Kaus, B. J. P.: LaMEM (Lithosphere and Mantle Evolution Model), <https://bitbucket.org/bkaus/lamem/src/master/>, 2016.
- Ramandi, H. L., Mostaghimi, P., and Armstrong, R. T.: Digital rock analysis for accurate prediction of fractured media permeability, *Journal of Hydrology*, 554, 817 – 826, <https://doi.org/https://doi.org/10.1016/j.jhydrol.2016.08.029>, 2017.
- Ren, X., Zhao, Y., Deng, Q., Li, D., and Wang, D.: A relation of hydraulic conductivity – Void ratio for soils based on Kozeny-Carman
670 equation, *Engineering Geology*, 213, <https://doi.org/10.1016/j.enggeo.2016.08.017>, 2016.
- Revil, A. and Cathles III, L. M.: Permeability of shaly sands, *Water Resources Research*, 35, 651–662, <https://doi.org/10.1029/98WR02700>, 1999.
- Rintoul, M. D.: Precise determination of the void percolation threshold for two distributions of overlapping spheres, *Phys. Rev. E*, 62, 68–72, <https://doi.org/10.1103/PhysRevE.62.68>, 2000.
- 675 Sahimi, M.: *Heterogeneous Materials I: Linear Transport and Optical Properties*, *Interdisciplinary Applied Mathematics*, Springer New York, <https://books.google.de/books?id=Ex8RBwAAQBAJ>, 2006.

- Saxena, N., Mavko, G., Hofmann, R., and Srisutthiyakorn, N.: Estimating permeability from thin sections without reconstruction: Digital rock study of 3D properties from 2D images, *Computers & Geosciences*, 102, 79–99, <https://doi.org/10.1016/j.cageo.2017.02.014>, 2017.
- 680 Selvadurai, P. and Selvadurai, A.: On the effective permeability of a heterogeneous porous medium: the role of the geometric mean, *Philosophical Magazine*, 94, 2318–2338, <https://doi.org/10.1080/14786435.2014.913111>, 2014.
- Shabro, V., Kelly, S., Torres-Verdín, C., Sepehrnoori, K., and Revil, A.: Pore-scale modeling of electrical resistivity and permeability in FIB-SEM images of organic mudrock, *Geophysics*, 79, D289–D299, <https://doi.org/10.1190/geo2014-0141.1>, 2014.
- Suleimanov, B. A., Ismailov, F. S., and Veliyev, E. F.: Nanofluid for enhanced oil recovery, *Journal of Petroleum Science and Engineering*, 78, 431–437, <https://doi.org/10.1016/j.petrol.2011.06.014>, 2011.
- 685 Taheri, S., Ghomeshi, S., and Kantzas, A.: Permeability calculations in unconsolidated homogeneous sands, *Powder Technology*, 321, 380–389, <https://doi.org/10.1016/j.powtec.2017.08.014>, 2017.
- Takeuchi, S., Nakashima, S., and Tomiya, A.: Permeability measurements of natural and experimental volcanic materials with a simple permeameter: toward an understanding of magmatic degassing processes, *Journal of Volcanology and Geothermal Research*, 177, 329–339, <https://doi.org/10.1016/j.jvolgeores.2008.05.010>, 2008.
- 690 Thorat, I. V., Stephenson, D. E., Zacharias, N. A., Zaghbi, K., Harb, J. N., and Wheeler, D. R.: Quantifying tortuosity in porous Li-ion battery materials, *Journal of Power Sources*, 188, 592–600, <https://doi.org/10.1016/j.jpowsour.2008.12.032>, 2009.
- Torquato, S.: *Random Heterogeneous Materials: Microstructure and Macroscopic Properties*, Interdisciplinary Applied Mathematics, Springer New York, <https://books.google.de/books?id=g0kAnwEACAAJ>, 2013.
- Van der Marck, S. C.: Network Approach to Void Percolation in a Pack of Unequal Spheres, *Phys. Rev. Lett.*, 77, 1785–1788, <https://doi.org/10.1103/PhysRevLett.77.1785>, 1996.
- 695 Wadsworth, F. B., Vasseur, J., von Aulock, F. W., Hess, K.-U., Scheu, B., Lavallée, Y., and Dingwell, D. B.: Nonisothermal viscous sintering of volcanic ash, *Journal of Geophysical Research: Solid Earth*, 119, 8792–8804, <https://doi.org/10.1002/2014JB011453>, 2014.
- Wadsworth, F. B., Vasseur, J., Scheu, B., Kendrick, J. E., Lavallée, Y., and Dingwell, D. B.: Universal scaling of fluid permeability during volcanic welding and sediment diagenesis, *Geology*, 44, 219–222, <https://doi.org/10.1130/G37559.1>, 2016.
- 700 Wang, D., Han, D., Li, W., Zheng, Z., and Song, Y.: Magnetic-resonance imaging and simplified Kozeny-Carman-model analysis of glass-bead packs as a frame of reference to study permeability of reservoir rocks, *Hydrogeology Journal*, 25, 1465–1476, <https://doi.org/10.1007/s10040-017-1555-7>, 2017.
- Warren, J. E. and Price, H. S.: Flow in Heterogeneous Porous Media, *Society of Petroleum Engineers Journal*, 1, 153–169, <https://doi.org/10.2118/1579-G>, 1961.
- 705 Waxman, M. H. and Smits, L. J. M.: Electrical Conductivities in Oil-Bearing Shaly Sands, *Society of Petroleum Engineers Journal*, 8, 107–122, <https://doi.org/10.2118/1863-A>, 1968.
- Wu, M., Xiao, F., Johnson-Paben, R. M., Retterer, S. T., Yin, X., and Neeves, K. B.: Single- and two-phase flow in microfluidic porous media analogs based on Voronoi tessellation, *Lab Chip*, 12, 253–261, <https://doi.org/10.1039/C1LC20838A>, 2012.
- Wyllie, M. R. J. and Gregory, A. R.: Fluid Flow through Unconsolidated Porous Aggregates, *Industrial & Engineering Chemistry*, 47, 1379–1388, <https://doi.org/10.1021/ie50547a037>, 1955.
- 710 Yoshimura, S. and Nakamura, M.: Fracture healing in a magma: An experimental approach and implications for volcanic seismicity and degassing, *Journal of Geophysical Research: Solid Earth*, 115, <https://doi.org/10.1029/2009JB000834>, 2010.
- Zhang, H., Nikolov, A., and Wasan, D.: Enhanced Oil Recovery (EOR) Using Nanoparticle Dispersions: Underlying Mechanism and Imbibition Experiments, *Energy & Fuels*, 28, 3002–3009, <https://doi.org/10.1021/ef500272r>, 2014.